GSK3 inhibition ameliorates the abnormal contractility of Newfoundland ACM patient iPSC-cardiomyocytes

Rebecca Noort[1], Wesam Salman[1], Zachary Porter[1], Hooman Sadighian[1], Camila Fuchs[1], Ursula Braun[1], David Pace[2], Thomas Belbin[1,3], Kathleen Hodgkinson[4], Jessica Esseltine[1#]

[1]Division of BioMedical Sciences, Faculty of Medicine. Memorial University of Newfoundland. St. John's, Canada A1B 3V6

[2]Discipline of Surgery, Faculty of Medicine. Memorial University of Newfoundland. St. John's, Canada A1B 3V6

[3]Discipline of Oncology, Faculty of Medicine. Memorial University of Newfoundland. St. John's, Canada A1B 3V6

[4]Division of Population Health and Applied Health Sciences, Faculty of Medicine. Memorial University of Newfoundland. St. John's, Canada A1B 3V6

[#]To whom correspondence can be addressed: jesseltine@mun.ca. Tel:1-709-864-3388

Keywords: Arrhythmogenic Cardiomyopathy, Transmembrane Protein 43, human pluripotent stem cells, cardiomyocytes, calcium imaging, CRISPR-Cas9 gene editing.

Abstract

Arrhythmogenic Cardiomyopathy (ACM) is clinically characterized by ventricular arrhythmias causing sudden cardiac death and fibrofatty replacement of the myocardium leading to heart failure. One form of ACM is highly prevalent in the Canadian Province of Newfoundland and Labrador (NL) and has earned the moniker, The “Newfoundland Curse”. This ACM in NL patients is often caused by a fully penetrant heterozygous missense mutation in the *TMEM43* gene (*TMEM43* c.1073C>T; TMEM43 p.S358L). Although the causative mutation has been identified, little is known about the function of the TMEM43 protein in cardiomyocytes, how the TMEM43 p.S358L mutation contributes to the development of arrhythmias, or why the disease is more severe in males than females. To explore the role of TMEM43 in cardiomyocyte function, we generated induced pluripotent stem cells (iPSCs) from 2 severely affected male Newfoundland ACM (TMEM43 p.S358L) patients. CRISPR-Cas9 was used to genetically “repair” the heterozygous *TMEM43* mutation in ACM patient iPSCs or for *TMEM43* gene knockout. ACM patient iPSC-cardiomyocytes with the TMEM43 p.S358L mutation display pro-arrhythmogenic phenotypes *in vitro* with significantly elevated contraction rates and altered calcium handling, although no obvious gross abnormalities were observed across several major intracellular organelles. TMEM43 protein abundance and half-life appears unchanged in ACM iPSC-CMs where 50% of the TMEM43 protein is WT and 50% is mutant. Gene expression analysis of ACM iPSC-CMs shows an increase in genes related to signaling and metabolism. Importantly, the pro-arrhythmic tendencies of ACM patient iPSC-CMs can be ameliorated with transient GSK3 inhibition.

Introduction

Arrhythmogenic Cardiomyopathy (ACM) is a category of related heart diseases featuring both ventricular arrhythmias causing sudden cardiac death and cardiomyopathy leading to heart failure[1]. About 60% of ACM cases have known genetic links across at least 13 different genes[2, 3]. ACM is often associated with the dysfunction of the desmosomes, which provide strength to the cardiac muscle. When the desmosomes break down, the myocardium cannot withstand the pressures exerted during beating, causing cardiomyocytes to break apart and die[1]. Cardiomyocyte electrical coupling via gap junctions is subsequently compromised when non-excitable fibrous tissue invades the damaged myocardium leading to ventricular arrhythmia. Other ACM pathogenic variants involve various calcium handling proteins as well as nuclear envelope proteins and linker of nucleoskeleton and cytoskeleton (LINC) complex[4]. In 2008, researchers at Memorial University of Newfoundland found an autosomal dominant mutation in the *TMEM43* gene (c.1073C>T, p.S358L) within a cluster of patients suffering from ACM[5, 6]. The same *TMEM43* mutation was subsequently reported in some European countries including the UK[7], Germany[8] and Denmark[9]. This pathogenic gene variant is fully penetrant, meaning that every individual who inherits this disease-causing allele will develop at least one clinical feature of ACM[6, 10]. Since TMEM43 p.S358L-linked ACM is an autosomal dominant disorder, children born into these families have a 50% risk of inheriting the disease-causing *TMEM43* allele. ACM is much worse in males than females: 50% of untreated males die by 40 years, 80% by 50 years (5% and 20% respectively for females)[1, 10]. Along with sex, the greatest risk factor for severe disease presentation is exercise[11-13]. This risk has lead to NL pediatric cariology supporting the

restriction of high impact sports for children with the TMEM43 p.S358L pathogenic variant long before they become symptomatic[13]. Primary ACM treatment for TMEM43 p.S358L ACM individuals is an Implantable Cardioverter Defibrillator (ICD) which monitors heart rate and discharges when a lethal arrhythmia is detected. ICD treatment has added an average 18 years of life to ACM patients compared to their untreated ancestors[5]. A large population of individuals with the TMEM43 p.S358L variant and their siblings and relatives born at an *apriori* 50% risk are ascertained in NL, with extensive clinical data over several generations.

Although TMEM43 p.S358L is a cause of ACM, we know very little regarding the function of TMEM43 protein or how *TMEM43* pathogenic variant compromises cardiomyocyte function. Here we generated and characterised induced pluripotent stem cell-cardiomyocytes (iPSC-CMs) from 2 severely affected male Newfoundland ACM patients with the autosomal dominant TMEM43 p.S358L mutation. iPSCs are ideal for disease modeling as they are of human origin, are patient-specific, amenable to genetic manipulation, and can differentiate into various terminal cell types. Unaffected familial controls together with isogenic “repair” iPSCs revealed that ACM iPSC-CMs exhibit profound pro-arrhythmic tendencies that can be ameliorated with GSK3 inhibition. The patient-oriented nature of this research will help inform some of the most fundamental mechanisms of cardiomyocyte dysfunction in patients with TMEM43 p.S358L pathogenic variant.

Material and Methods

Human Ethics

These studies are approved by the Newfoundland and Labrador Human Research Ethics Board (HREB #2018.210 & 2020.301). All approvals are reviewed and renewed annually.

Human AD293 Cell Culture

AD293 cells (Cat # 240085, Agilent, Santa Clara, USA) were cultured in Dulbecco's Modified Eagle Medium (DMEM; Cat # 319-015-CL, Wisent, St-Bruno, CAN) supplemented with (10% v/v) Fetal Bovine Serum (FBS) (Cat # 10437028, Fisher Scientific, Ottawa, CAN) and housed at 37°C and 5% CO_2. The cells were passaged once they reached 70-80% confluency in the flask via Trypsin-EDTA (0.05% Trypsin, Cat # 325-044-EL, Wisent; 0.53 mM EDTA, Cat # AM9260G, ThermoFisher Scientific, Waltham, USA).

Human Induced Pluripotent Stem Cell Culture

The female control iPSC cell line was derived from dermal fibroblasts taken from a 32-year old Caucasian female with no known illnesses[25]. iPSCs were maintained in either Essential 8 medium (E8) (Cat # A1517001, ThermoFisher Scientific) or mTeSR™-Plus (Cat # 100-0276, STEMCELL Technologies, Vancouver, CAN) in 6-well plates pre-coated with Geltrex (Cat # A1413302, ThermoFisher Scientific). Cells received daily media changes and were passaged every 4-5 days as aggregates using 0.5 mM EDTA in DPBS (Cat # AM9260G, ThermoFisher Scientific). Cell aggregates were gently scraped off the bottom of the well and re-seeded onto a new Geltrex-coated dish.

ACM Patient Dermal Biopsy and Primary Fibroblast Isolation

The patient samples used in this study included two severely affected male ACM patients from NL as well as one unaffected brother. Primary fibroblasts were isolated via outgrowth from dermal punch biopsies. Primary fibroblasts were cultured on 0.1% gelatin coated dishes in DMEM supplemented with FBS (20% v/v). Cells were maintained in an incubator at 37°C and 5% CO_2. The cells were passaged with Trypsin-EDTA once they reached confluency. Passage 2-3 primary dermal fibroblasts were used for iPSC reprogramming.

Human Induced Pluripotent Stem Cell Reprogramming & Characterization

Dermal fibroblasts were reprogrammed using a ReproRNA™-OKSGM Kit (Cat # 05903, STEMCELL Technologies) according to the manufacturer's instructions. Resulting iPSC colonies were picked and transitioned onto Geltrex-coated plates with Essential 8 medium. At passage 8, iPSC lines were tested for mycoplasma contamination (Mycoplasma PCR Detection Kit; Cat # G238, abm, Richmond, CAN), normal copy number at mutation hotspots (hPSC Genetic Analysis Kit; Cat # 07550, STEMCELL Technologies), and >90% expression undifferentiated state markers (TRA-1-60, SSEA4, OCT4; see antibodies in Table 1). *TMEM43* variant status in the iPSCs was confirmed relative to the starting fibroblast population by Sanger Sequencing a PCR amplicon flanking the c.1073 mutation site. Only resulting iPSC lines that passed all quality checks were used for experiments.

Table 1 Antibodies and Dyes used in Western Blot, Immunofluorescence, & Flow Cytometry

Marker	Supplier	Catalog #	Host Species	IF	Western Blot	FC
6X-His Tag	ThermoFisher Scientific	MA5-33032	rabbit		1:1000	
AKT (pan)	Cell Signaling Technology, (Danvers, USA)	4691	rabbit		1:1000	
Calnexin	Cell Signaling Technology	2679	rabbit		1:1000	
Calnexin	ThermoFisher Scientific	MA3-027	mouse		1:1000	
Connexin 43	MilliporeSigma (Burlington, USA)	C6219	rabbit	1:1000	1:5000	
cTNT (cardiac troponin T)	Abcam (Cambridge, GBR)	ab8295	mouse	1:800		0.1 uL/test
Emerin	Abcam	ab204987	mouse		1:1000	
Emerin	Cell Signaling Technology	30853	rabbit		1:1000	
FLAG Tag	MilliporeSigma	F1804	mouse		1:1000	
FLAG Tag	Cell Signaling Technology	14793	rabbit		1:1000	
GAPDH	MilliporeSigma	MAB374	mouse		1:5000	
Lamin A/C	Abcam	ab238303	mouse	1:1000	1:1000	
MLC2V	Abcam	ab79935	rabbit	1:500		
N-Cadherin	BD Biosciences (Franklin Lakes, USA)	610921	mouse	1:500	1:2000	
OCT4 BrilliantViolet™421	BioLegend (San Diego, USA)	653712	mouse			0.5 uL/test
Phospho-AKT (Ser473)	Cell Signaling Technology	4060	rabbit		1:1000	
Phospho-AKT (Thr308)	Cell Signaling Technology	13038	rabbit		1:1000	
Phospho-c-Raf (Ser259)	Cell Signaling Technology	9421	rabbit		1:1000	
Phospho-GSK-3β (Ser9)	Cell Signaling Technology	5558	rabbit		1:1000	
Phospho-PDK1 (Ser241)	Cell Signaling Technology	3438	rabbit		1:1000	
Phospho-PTEN (Ser380)	Cell Signaling Technology	9551	rabbit		1:1000	
Plakoglobin (gamma catenin)	Abcam	ab231304	mouse	1:1000		
SERCA2 / ATP2A2	Cell Signaling Technology	9580	rabbit		1:1000	
SSEA4 AF647	BioLegend	330408	mouse			0.2 uL/test
TMEM43	Abcam	ab184164	rabbit		1:2000	

TRA-1-60-R	BioLegend	330614	mouse			2 uL/test
Goat-anti-mouse IgG, HRP-linked	ThermoFisher Scientific	31430	Goat		1:5000	
Goat-anti-rabbit IgG, HRP-linked	Cell Signaling Technology	7074	Goat		1:1000	
donkey-anti-mouse AF555	ThermoFisher Scientific	A31570	Donkey	1:1000		
donkey-anti-rabbit AF488	ThermoFisher Scientific	A21206	Donkey	1:1000		
goat-anti-mouse AF647	ThermoFisher Scientific	A32728	Goat	1:1000	1:5000	1:3000
goat-anti-rabbit AF488	ThermoFisher Scientific	A78953	Goat		1:5000	
Hoechst 33342	FisherScientific	H3570	Dye	1:1000		
Phalloidin-647	Cell Signaling Technology	8940	Dye	1:20		
Zombie-Aqua fixable viability dye	BioLegend	423101	Dye			1:200
Zombie-NIR fixable viability dye	Biolegend	423105	Dye			1:1000
Mouse IgG1 isotype control	Cell Signaling Technology	5415	mouse			

TMEM43 CRISPR-Cas9 Genetic Ablation

TMEM43 knock-out AD293 and iPSC cell lines were created using CRISPR-Cas9 genetic ablation as described previously[29,30]. Two single guide RNAs (sgRNA) targeting human *TMEM43* were designed using the Sanger Institute CRISPR finder (http://www.sanger.ac.uk/htgt/wge/) (Sanger sgRNA ID 950611662 (5´-TGGCGCCTTACGGACATCCA-3´); Sanger sgRNA ID 950611647 (5´-ACGGCAACCTCATTGGCTGA-3´). The sgRNAs were selected based on their predicted efficiency and low predicted off-target effects. The two sgRNAs were cloned into either the pSpCas9(BB)-2A-GFP (PX458) plasmids (Addgene, Cambridge, USA)[31]. The human AD293 and iPSC cell lines were transfected using the Mirus TransIT®-LT1 Transfection Reagent (Cat # MIR 2300, Mirus Bio LLC, Madison, USA) according to the manufacturer's instructions. After transfection, GFP-expressing cells were sorted using fluorescence-

activated cell sorting (FACS) on a MoFlo Astrios Cell Sorter with a 488 nm laser (Beckman Coulter, Brea, USA). TMEM43 protein ablation was confirmed via Western blotting.

TMEM43 p.358L CRISPR-Cas9 Isogenic Repair

ACM iPSCs harbouring the pathogenic *TMEM43* c.1073T (p.358L) allele were corrected to *TMEM43* c.1073C (p.358S) to create isogenic repair iPSCs. CRISPR-Cas9 gene editing was performed according to STEMCELL Technologies' *Genome Editing of Human Pluripotent Stem Cells Using the ArciTect™ CRISPR-Cas9 System* Technical Document # 27084 Version 3.0.1 FEB 2022 with slight modification in conjunction with the Neon™ Electroporation System (Cat # MPK5000, ThermoFisher Scientific).

A gRNA proximal to the *TMEM43* c.1073T mutation site was identified with the Sanger Institute CRISPR finder (CRISPR ID 9506163618 (5'-CACGGTCAGCAGGGTCAGCG-3´)) and was modified by changing the 3' guanine to an adenine to make the gRNA specific to the pathogenic *TMEM43* allele. Analysis of the gRNA with IDT's CRISPR-Cas9 guide RNA design checker reveals no probable off-target effects. A 108 nt ssODN (single stranded oligodeoxynucleotide) with symmetrical homology arms was created using IDT's Alt-R™ CRISPR HDR Designing Tool and the positive strand polarity was selected based on principles described[14]. The ssODN contains three altered nucleotides to (A) correct *TMEM43* c.1073T to c.1073C, (B) destroy the PAM sequence after cutting, and (C) ablate an MlsI digest site.

Low-passage ACM iPSCs with normal chromosome copy number were subjected to CRISPR-Cas9 gene editing by electroporation with an RNP (ribonucleoprotein) complex and the ssODN along with a GFP-containing plasmid to facilitate identification

of successfully transfected cells. The electroporation reaction consists of 1.248 µM Cas9, 4 µM sgRNA, 3.33 µM ssODN, 0.033 µg/µL pEGFP-N1 plasmid, and 66,000 single cell iPSCs/µL. The mixture was loaded into a Neon™ 10 µL pipet tip, electroporated with 1 pulse at 1200V for 30 ms, plated into a single well of a Geltrex-coated 24 well plate containing mTeSR™ Plus + CloneR™2 (Cat # 100-0691STEMCELL Technologies) + 0.1% (v/v) Alt-R(T) HDR Enhancer V2 reagent, and incubated overnight at 37°C at 5% CO_2.

The following day (14-20 hours after electroporation), the cells were singularized using Accutase and GFP+ cells were isolated by FACS. Sorted cells were plated at clonal density (5-80 cells/cm^2) onto Geltrex-coated plates containing mTeSR™ Plus and CloneR™2 for three days followed by mTeSR™ Plus thereafter. Well-isolated iPSC colonies were picked and assayed for the desired gene edit by MlsI restriction digest assay and by Sanger sequencing (The Center for Applied Genomics, SickKids Hospital, Toronto, Canada). Resulting isogenic repair iPSCs that passed all quality checks as described above (see Human Induced Pluripotent Stem Cell Reprogramming & Characterization) were used for subsequent experiments.

Cardiomyocyte Differentiation & Replating

iPSCs were differentiated into contracting ventricular cardiomyocytes using a commercially available kit (STEMdiff™ Ventricular Cardiomyocyte Differentiation kit, Cat # 05010, STEMCELL Technologies). iPSCs were passaged into single cells using Accutase (Cat # A1110501, Thermo) at a cell density of 2.0 - 2.5 x 10^5 cells/cm^2 into the desired vessel. Once the cells reached >95% confluency, cardiomyocyte differentiation

was initiated as per the manufacturer's instructions. Beating cardiomyocytes were fed every other day with STEMdiff™ Maintenance Medium (Cat # 05020) until day 40.

Contracting cardiomyocytes were singularized for downstream applications like flow cytometry, calcium imaging, and fluorescence microscopy. Cells were incubated in a solution of 2% collagenase type II (Cat # LS004174, Worthington Biochem, Lakewood, USA), prepared in Hanks Balanced Salt Solution (HBSS; Cat # 14025092, ThermoFisher Scientific) to detach the cardiomyocytes from the growth surface. The collagenase solution was removed and the cells were singularized using 0.25% trypsin/ 0.5 mM EDTA followed by gentle trituration. Cardiomyocytes were pelleted to remove the trypsin and replated onto Geltrex-coated dishes containing STEMdiff™ Maintenance Medium + 10 uM Y-27632. The day after replating, medium was changed to STEMdiff™ Maintenance Medium without Y-27632 and cardiomyocytes were permitted to re-establish contractions (2-4 days) before use in downstream assays. Generally, iPSC-cardiomyocytes were used for experimentation after 40 days of contraction *in vitro*.

Cycloheximide Chase (TMEM43 Half-life)

AD293 cells and iPSCs were seeded at a density of 2.5 x 10^4 cells/cm^2 and treated with 25 µM of cycloheximide (Cat # C1988, Sigma-Aldrich, St. Louis, USA) in their respective culture media for the indicated time points. Contracting cardiomyocytes were treated with 100 µM cycloheximide prepared in STEMdiff™ Maintenance Medium for up to 24 hours. Cell lysates were made from each experimental condition, and protein levels were determined using SDS-PAGE and Western blotting as described below.

Subcellular Fractionation

Subcellular fractionation was used to sequentially isolate cytosolic, membrane-bound, and nuclear protein fractions as described[15] with slight modification. All lysis buffers were supplemented with phosphatase inhibitors NaF (10 mM) and Na_3VO_4 (1 mM) along with 1X protease inhibitor cocktail (ROCHE cOmplete Protease Inhibitor Cocktail Cat # 1169498001, MilliporeSigma). Incubation in cytosolic lysis buffer was performed for 30 minutes at 4°C on a rotator. Benzonase was added to the nuclear lysis buffer at 260 U/mL and nuclear protein extraction was performed for 1 hour at 4°C on a rotator. Resulting protein fractions were prepared for SDS-PAGE and Western Blotting as described below.

Co-Immunoprecipitation

C-terminal TMEM43 FLAG constructs were created by cloning TMEM43 p.358S or p.358L into a p3xFLAG-CMV-14 expression vector (Cat # E7908, MilliporeSigma). Similarly, a C-terminal TMEM43 Myc-His fusion construct was made by cloning wild type TMEM43 into a pcDNA3.1+ expression vector. NorClone Biotech Laboratories (London, CAN) created the constructs. *TMEM43-/-* AD293 cells (described above) were transfected with combinations of these plasmids using Mirus TransIT®-LT1 Transfection Reagent according to the manufacturer's instructions. Approximately 48 hours after transfection, cells were lysed in ice-cold lysis buffer consisting of 150 mM NaCl; 50 mM Tris pH 8.0; 0.1% Triton X-100; 2 µg/mL Leupeptin; 2 µg/mL Aprotinin; 10 mM NaF; 1 mM Na_3VO_4; 0.02% NaN_3. Cell lysate was immunoprecipitated using the indicated antibodies conjugated to Dynabeads™ Protein G (Cat # 10003D, ThermoFisher Scientific).

Immunoprecipitated proteins were run on SDS-PAGE gels and evaluated by Western blot as described below.

SDS-PAGE & Western Blot

Cells were lysed in ice-cold lysis buffer supplemented with protease and phosphatase inhibitors (150 mM NaCl; 50 mM Tris pH 8.0; 1.0% Triton X-100; 2 µg/mL Leupeptin; 2 µg/mL Aprotinin; 10 mM NaF; 1 mM Na_3VO_4; 0.02% NaN_3). Soluble protein concentration was determined using the Pierce BCA Protein Assay Kit (Cat # PI23225, ThermoFisher Scientific) as per the manufacturer's instructions. Proteins were separated via sodium dodecyl sulfate-polyacrylamide gel electrophoresis (SDS-PAGE) on 7.5% polyacrylamide gels or 4-20% gradient gels (Cat # 4561094 Bio-Rad, Hercules, USA). The gel was then transferred to a nitrocellulose membrane with a pore size of 0.45 µm (Cat # 1620115, Bio-Rad). The nitrocellulose membrane was incubated in primary antibody diluted in blocking buffer (3% w/v milk in pH 7.6 Tris Buffered Saline with TWEEN® 20 (TBST)): 15.23 mM Tris HCl, 4.62 mM Tris base, 150 mM NaCl, and 0.1% TWEEN® 20. Primary and secondary antibodies used for Western blot were prepared in block buffer as indicated in Table 1. Where used, HRP-conjugated secondary antibodies were visualized using Clarity™ Western ECL Substrate (Cat # 1705061, Bio-Rad) and blot images captured using the ChemiDoc™ MP Imaging System (Cat # 12003154 Bio-Rad). Immunoblots were analyzed by densitometry using FIJI software (ImageJ 1.52p). Every immunoblot was normalized to the house-keeping protein glyceraldehyde 3-phosphate dehydrogenase (GAPDH) when performing densitometric analysis.

Confocal Microscopy

Cells cultured on #1.5 glass coverslips or Nunc™ Lab-Tek™II chamber slides (Cat # 154453, ThermoFisher Scientific) were washed with DPBS and fixed in 10% normal buffered formalin (Cat # HT501128, MilliporeSigma) for 10 minutes at room temperature. Fixed cells were permeabilized in PBS-T (DBPS + 0.1% TWEEN®20) for 20 minutes followed by 0.1% Triton-X-100 in DPBS for 10 minutes. Primary antibodies were diluted in PBS-T + 5% BSA (Cat # 800-095-EG, Wisent) + 0.05% NaN_3 and incubated overnight at 4°C. Secondary antibodies and dyes (prepared in PBS-T were incubated at room temperature for 2 hours. Antibodies and stains used for immunofluorescence are indicated in Table 2. The slides were mounted using mowial®488 reagent with 1,4-diazabicyclo[2.2.2]octane (DABCO) antifade compound as described by Cold Spring Harbor Protocols[16].

Immunofluorescence confocal images were taken on a Zeiss LSM 900 with Airyscan 2 fitted with a 63X/1.4NA oil immersion lens and the following lasers: 405 nm, 488 nm, 561 nm, 640 nm. All images taken were analyzed and processed using FIJI software.

Electron Microscopy

Contracting cardiomyocytes were rinsed with DPBS and scraped as a single sheet from the culture surface and fixed in Karnovsky's fixative overnight. Fixed samples were processed for transmission electron microscopy according to standard methods. Images were captured on a Tecnai Spirit Transmission electron microscope with a 4-megapixel AMG digital camera.

Flow Cytometry

Single cell suspensions were prepared for flow cytometry and stained with Zombie fixable viability dyes and antibodies as shown in Table 2. Samples were analyzed on a CytoFLEX flow cytometer (Beckman Coulter) equipped with 405 nm, 488 nm, and 638 nm lasers. Analysis was performed with FlowJo™ v.10.3 Software. UltraComp eBeads™ Plus Compensation Beads (Cat # 01-3333-41, Thermo) labeled with fluorescent-tagged antibodies were used for compensation. Gate placement was determined using fluorescence minus one (FMO) or secondary antibody only controls as appropriate.

Live Cell Calcium Imaging

Contracting iPSC-CMs cultured on high end microscopy µ-slides (Cat # 80806, Ibidi, DEU) were incubated with 10 µM Fluo-4 AM dye (Cat # F14201, Thermo) in cardiomyocyte maintenance medium for 15 minutes at 37°C and 5% CO_2. After incubation, iPSC-CMs were washed with HBSS (Thermo) and fresh cardiomyocyte maintenance medium was then added to wells. Calcium transients were captured on a Zeiss LSM 900 with Airyscan 2 with a 20X/0.8NA objective and 488 nm laser. The cells were housed in a humidified 37°C chamber with 5% CO_2 throughout image acquisition.

Drug Treatments

After 40 days of contraction *in vitro*, iPSC-cardiomyocytes were stimulated with 1 µM isoproterenol before calcium imaging. Cells were pre-treated with the GSK3 inhibitor CHIR99021 (2 µM) (Cat # 13122, Cayman Chemicals, Ann Arbor, USA) for ~20 days until analysis on Day 40.

Calcium Imaging Analysis

Images taken over a 20-30 second time period were analyzed by FIJI with the “plot profile” to generate a list of xy coordinates for Fluo-4 AM intensity over time. These values were processed using Origin® 2023 software (OriginLab Corporation, Northhampton, USA) with the calcium transient app to determine F/F0 and other parameters describing the shape of each calcium transient. Data were plotted using GraphPad Prism version 9.4.1 (GraphPad Software Inc, San Diego, USA).

RNA Extraction and Sequencing

Total RNA was isolated using Invitrogen PureLink RNA Mini Kit (Cat # 12183020, ThermoFisher Scientific) with on-column DNase I treatment (Cat# 12185010, ThermoFisher Scientific) according to the manufacturer’s instructions. RNA concentration and quality were measured with a NanoDrop™ 2000 spectrophotometer (Cat# ND-2000, ThermoFisher Scientific) where an A260/280 ratio >2.0 indicated high quality RNA. Purified RNA was sequenced at Genome Quebec on an Illumina NovaSeq 600 S4 PE100.

Whole transcriptome analysis of ACM patient iPSC-cardiomyocytes using RNA sequencing.

Whole transcriptome analysis of gene expression differences in iPSC-CMs was carried out by RNA sequencing on a Illumina NovaSeq 6000 S4 PE100 (Genome Quebec). Paired end 100bp reads were assessed for quality control using FastQC (version 0.11.9; http://www.bioinformatics.babraham.ac.uk/projects/fastqc/[17]. Reads were aligned to the Human hg38 reference genome using RNA-Star (Galaxy Version 2.7.8a) with default settings[18] and transcripts were counted using featureCounts (Galaxy version 2.0.1)[19]. Differential expression of genes between ACM patient and matched Control cells were based on a model using the negative binomial distribution with DeSeq2 (Galaxy Version 2.11.40.7), with a Benjamini-Hochberg adjusted p-value of less than 0.05[20].

Identification of overrepresented groups of genes was carried out using goseq (Galaxy Version 1.44.0)[21]. The three Gene Ontology (GO) categories were GO:MF (Molecular Function), GO:CC (Cellular Component), GO:BP (Biological Process). Distributions of the numbers of members of a category amongst the differentially expressed genes were determined by the Wallenius non-central hypergeometric distribution. P-values for over representation of the GO term in the differentially expressed genes were adjusted for multiple testing with the Benjamini-Hochberg procedure. Goseq was similarly applied for KEGG pathway-based enrichment of differentially expressed genes.

Statistical Analysis

All statistical analyses were performed using GraphPad Prism version 9.4.1 (GraphPad Software Inc, San Diego, USA). Bar graph data are presented as mean ± standard error values and violin plots show the median and quartile positions. When comparing two data sets, unpaired t-test was used to analyze data and determine significance. For data sets of three or more, one-way analysis of variance (ANOVA) with Tukey's post hoc multiple comparisons test was used to determine statistical significance. A p-value of less than 0.05 was considered significant in this study where not significant (ns) $p>0.05$, * $p\leq0.05$, ** $p\leq0.01$, *** $p\leq0.001$, and **** $p\leq0.0001$.

Results

ACM patient iPSC-cardiomyocytes exhibit pro-arrhythmic tendencies

In this study we reprogrammed iPSCs from 2 male NL ACM patients with the TMEM43 p.S358L heterozygous pathogenic variant. These individuals were selected based on a severe disease presentation: ICD discharge for sustained VT ≥ 240 bpm under age 35 years and a maintained history of appropriate discharges and progression of disease ultimately requiring heart transplant before the age of 40 (Table 2). We also reprogrammed iPSCs from one unaffected brother and included iPSCs from an unrelated healthy female donor. CRISPR-Cas9 genetic engineering was used to generate *TMEM43-/-* iPSCs as well as create isogenic control cells by "repairing" the TMEM43 p.S358L mutation in ACM patient iPSCs (Supplemental Figure 1 A-D).

Table 2. Patient-derived iPSC samples included in the study

Sample	TMEM43 Variant	Sex	Age at Biopsy (yrs)	# ICD Shocks	ICD Runs and ATP	Age at Heart Transplant (yrs)
ACM	WT / p.S358L	XY	49	>25	>50	36
Isogenic Repair	WT / WT	XY	-	-	-	-
Control (unaffected sibling)	WT / WT	XY	46	N/A	N/A	None
ACM	WT / p.S358L	XY	41	>15	>25	36
Control (unrelated healthy donor)	WT/WT	XX	33	N/A	N/A	None
TMEM43 knockout	-/-	XX	-	-	-	-
Abbreviations: ATP (antitachycardia pacing); ICD (implantable cardioverter defibrillator).						

All iPSC lines successfully differentiated into cardiomyocytes and routine testing was used to confirm high proportions of differentiated cells expressing the cardiomyocyte

marker cardiac troponin T (cTNT) and the ventricular myocyte marker myosin light chain 2V (MLC2V) (Supplemental Figure 1 E-G). It became immediately apparent that both ACM patient-derived iPSC-CM lines exhibited significantly higher contraction frequencies under basal conditions (Figure 1A, B, Supplemental videos). Indeed, our unaffected control iPSC-CMs contracted an average of 16.25 +/- 0.6226 (unaffected sibling) or 25.05 +/- 1.507 (unrelated control) times per minute while the ACM iPSCs contracted an average of 36.63 +/- 2.831 (patient #1) or 38.09 +/- 2.161 (patient #2). Interestingly, the isogenic “repair” iPSC-CMs also exhibited significantly higher contraction frequencies compared to either of our unaffected control lines (35.95 +/- 2.944). This increased contraction rate resulted in a significant decrease of nearly all of the calcium transient parameters tested, including time to peak, decay time, transient duration and time between maxima (Figure 1 D, E). Moreover, blinded scoring showed a dramatic increase in the number of pro-arrhythmic events from ACM patient iPSC-CM calcium traces compared to control or isogenic repair iPSC-CMs (Figure 1C).

Isoproterenol exacerbates the pro-arrhythmic tendencies of isogenic repair patient iPSC cardiomyocytes

Exercise is one of the largest contributors to severe disease in ACM patients with the TMEM43 p.S358L mutation. Therefore, we sought to determine whether mimicking exercise with the β-adrenergic receptor agonist isoproterenol would exacerbate the pro-arrhythmic tendencies that we observed in the unstimulated ACM patient iPSC-CMs (Figure 2). Surprisingly, we did not observe an increased proportion of pro-arrhythmic traces from ACM patient iPSC-CMs treated with 10 µM isoproterenol (Figure 2A, C). Isoproterenol treatment also did not significantly increase the contraction frequency of

ACM patient iPSC-CMs (Figure 2B), possibly because they were already contracting at such high rates that a further increase was simply impossible. Most surprisingly, however, was that isoproterenol treatment did increase the proportion of pro-arrhythmic calcium traces in the isogenic “repair” iPSC-CMs (Figure 2A, B, C). Even though these cells had the TMEM43 p.S358L mutation reverted back to wild type, isoproterenol treatment triggered higher contraction frequencies and pro-arrhythmic traces in these cells compared to either unstimulated “repair” iPSC-CMs or isoproterenol-treated control iPSC-CMs (Figure 2A, B, C).

ACM patient iPSC-CMs exhibit typical cellular organelle morphology

TMEM43 p.S358L and other human disease-causing TMEM43 mutations have been shown to disrupt TMEM43 protein trafficking and stability in different systems[22]. However, Western blot analysis showed no significant changes in TMEM43 protein abundance in control or ACM patient iPSC-CMs (Figure 3A, B). Cycloheximide treatment across several different human cell lines demonstrated that TMEM43 is a relatively long-lived protein with a half-life of longer than 24 hours, and that the half-life remained greater than 24 hours in ACM patient iPSC-CMs that express 50% wild type and 50% mutant TMEM43 protein (Figure 3C, D, Supplemental Figure 2A, B). Co-immunoprecipitation experiments in human AD293 cells demonstrate that TMEM43 self-oligomerizes both between WT-WT and WT-S358L (Supplemental Figure 2C). Finally, subcellular fractionation revealed that TMEM43 protein resides primarily in the membrane fraction of both control and ACM iPSC-CMs (Figure 3E, Supplemental Figure 2D). We tried to use immunofluorescence confocal microscopy to identify the subcellular localization of TMEM43 in control and ACM patient iPSC-CMs. Unfortunately, while all of the

commercially available TMEM43 antibodies we tested worked well for Western blot, none of them were suitable for immunofluorescence in our hands, exhibiting similar staining patterns in WT and *TMEM43-/-* cells (Supplemental Figure 3).

Several other ACM-causing mutations have been reported to impact various intracellular organelles including gap junctions, desmosomes, nuclear envelop proteins and others[2, 3]. Thus, we sought to determine whether any of these organelles were perturbed in our ACM patient iPSC-CMs. Subcellular fractionation showed no apparent alteration in the subcellular distribution of key intracellular proteins while Western blot analysis revealed that ACM iPSC-CMs express similar levels of total and phosphorylated Cx43 protein (Figure 3E, F). Similarly, electron microscopy and immunofluorescence confocal imaging both revealed little apparent differences in nuclear envelope, gap junctions, desmosomes, sarcomeres, Z-discs, mitochondria structure, or protein localization between the unaffected control and ACM patient iPSC-CMs (Figure 4, Supplemental Figures 4A & 5). Finally, flow cytometric analysis of the apoptosis marker cleaved caspase 3 (CC3) was used to determine whether ACM patient iPSC-cardiomyocytes exhibited increased apoptosis rates (Supplemental Figure 4B). We observed similarly low rates of CC3-positive cells across all of the cell lines examined (< 1%), suggesting that our ACM patient iPSC-cardiomyocytes do not exhibit increased apoptosis rates *in vitro*.

ACM patient iPSC-CMs exhibit altered expression of genes related to metabolism, signaling, and transmembrane transport.

Altered signal transduction has also been proposed as a mechanism of ACM associated with TMEM43 p.S358L[23]. However, we found no difference in key signaling

proteins within the AKT signaling axis between ACM patient and unaffected control iPSC-CMs, including phospho-AKT, phospho-GSK3β and others (Figure 5). Thus, RNAseq was used to further understand how gene expression is perturbed in ACM patient iPSC-CMs. We compared ACM patient iPSC-CMs to unaffected familial control after filtering for genes that were common between the ACM patient and the isogenic control samples (Figure 6A). Analysis of transcriptomic data using DESeq2 revealed a total of 574 differentially expressed genes with an adjusted p-value of less than 0.05 and a log fold change ($\log_2$FC) of at least 1 (or -1) (492 up-regulated, 82 down-regulated) (Figure 6B; Supplementary Data). We grouped differentially expressed genes along common biological themes using gene set enrichment analysis (GSEA) with gene ontology (GO) terms related to biological processes (BP), molecular function (MF), cellular component (CC), KEGG and reactome pathways (Figure 6C-F; Supplementary Data). Significantly enriched KEGG pathways included those associated with drug, porphyrin and retinol metabolism, as well as maturity onset diabetes of the young (Figure 6C). GO:BP was also enriched in categories related to metabolic processes while GO:MF was enriched in signaling receptor activity (Figure 6D, E). Differentially expressed genes in cellular components were over-represented in GO categories related to the plasma membrane, extracellular space and other cellular membrane compartments (Figure 6F). Most strikingly among the differentially expressed genes was the sheer number of solute carriers upregulated in our ACM patient iPSC-CMs compared to control. Indeed, 28 of the 492 upregulated genes (~5.7% of all upregulated genes; none in downregulated genes) belonged to the solute carrier class of proteins (Table 3).

Table 3. Solute carrier genes upregulated in ACM patient iPSC-CMs

Gene name	Fold Increase	Biological/Cellular Function	Predicted intracellular localization (Human Protein Atlas)
SLC26A3	**213.42**	Chloride anion exchanger	Apical membrane domain
SLC19A3	**140.07**	Thiamine transporter	Nucleoplasm, plasma membrane, cytosol
SLC17A1	**96.45**	sodium-dependent phosphate transporter	Golgi apparatus
SLC2A14	**60.99**	glucose transporter	Plasma membrane
SLC39A2	**49.45**	zinc transporter	Plasma membrane, cytoplasmic bodies
SLC17A4	**45.09**	membrane potential-dependent organic anion transporter	Membrane
SLCO2B1	**39.11**	Na+-independent transport of steroid sulfate conjugates	Membrane, intracellular
SLC39A5	**31.49**	Zinc transporter	Vesicles, nucleoplasm
SLC5A9	**25.47**	Electrogenic Na(+)-coupled sugar symporter	Actin filaments, cytosol
SLC7A7	**24.14**	light subunit of a cationic amino acid transporter	Membrane
SLC15A1	**20.70**	hydrogen peptide cotransporter	Nucleoplasm, cytosol
SLC27A2	**15.94**	long-chain fatty acid transporter activity	Membrane
SLC38A4	**9.49**	cotransports neutral amino acids and sodium ions	Membrane
SLC51A	**8.75**	bile acid export	Membrane, intracellular
SLC6A11	**8.63**	sodium- and chloride-dependent transport of gamma-aminobutyric acid (GABA)	Nucleoplasm, vesicles
SLC52A3	**7.59**	riboflavin transporter	Membrane
SLCO2A1	**7.44**	prostaglandin transporter	Membrane
SLC22A31	**7.39**	organic ion transporter	Membrane
SLC30A10	**5.71**	manganese efflux transporter	Membrane
SLC28A3	**5.68**	concentrative nucleoside transporter	Membrane
SLC2A2	**5.47**	D-glucose transmembrane transporter activity	Plasma membrane
SLC26A2	**4.55**	Na(+)-independent sulfate/chloride antiporter	Vesicles
SLC38A5	**4.23**	cotransports neutral amino acids and sodium ions	Vesicles, plasma membrane
SLC16A4	**3.94**	monocarboxylic acid transporter	Microtubules, cytokinetic bridge
SLC44A3	**3.62**	Choline transporter-like protein	Membrane, intracellular
SLC1A1	**3.49**	high-affinity glutamate transporter	Membrane
SLC9A3R1	**3.26**	Sodium-hydrogen antiporter 3 regulator 1	Plasma membrane, vesicles, centriole
SLC1A3	**2.52**	high affinity glutamate transporter	Nucleoli, vesicles

ACM iPSC-CM pro-arrhythmic tendencies can be ameliorated with GSK3 inhibition

While we observed no changes in phospho-GSK3β protein expression, treatment with the GSK3 inhibitor CHIR99021 had a profound effect on ACM iPSC-CMs. Indeed, GSK3 inhibition significantly improved every metric we evaluated including reduced contraction frequency, extended transient duration, and vastly reduced pro-arrhythmic traces in blinded scoring (Figure 7A-E). Furthermore, GSK3 inhibition also positively impacted many aspects of the isogenic “repair” cells (Figure 7F-J).

Discussion

This is the first comprehensive characterization of iPSC-cardiomyocytes from NL ACM patients harboring the TMEM43 p.S358L mutation. There are 27 ACM families spanning 12 generations in NL that carry the TMEM43 p.S358L founder mutation[6, 10, 24]. The TMEM43 p.S358L is fully penetrant, in that every person who inherits the disease-causing allele will develop features of ACM once entering adulthood[5, 6, 10, 11, 24, 25]. The worst outcome is sudden cardiac death in young, previously asymptomatic individuals. However, clinical presentations in ACM patients can greatly vary, ranging from minor symptoms to heart failure requiring transplant. The biggest contributor to disease variability is sex: 80% of untreated males and 20% of untreated females die by age 50[1]. Along with sex, the greatest risk factor for severe disease presentation is exercise[11-13]. Symptom-free children with the TMEM43 p.S358L variant are advised to limit high impact, (particularly competitive) sports in NL. Because *TMEM43*-associated ACM is autosomal dominant, children have a 50% risk of inheriting the disease from an affected parent and are screened for the disease-causing variant in childhood

The molecular function of TMEM43 protein is poorly understood and how the TMEM43 p.S358L pathogenic variant causes ACM is virtually unknown. Uncovering the fundamentals of the TMEM43 protein life cycle and localization are essential to understanding the molecular role of TMEM43 function. *In silico* modelling and immunoprecipitation studies have proposed that TMEM43 self oligomerizes[23, 26]. Indeed, our co-immunoprecipitation results confirm oligomerization of wildtype TMEM43 with itself and also with TMEM43 p.S358L. Given this interaction, it is possible that mutant TMEM43 could negatively impact the function of the wild type isoform in cardiomyocytes. We also

find that the half-life of both wild type TMEM43 and TMEM43 p.S358L is greater than 24 hours in iPSC-CMs suggesting that the p.S358L mutation does not adversely impact protein expression or stability within that timeframe. Furthermore, while widely referred to as a nuclear envelope protein, TMEM43 has been shown to localize to the endoplasmic reticulum (ER), the intercalated disc, and gap junctions in different model systems[22, 27, 28]. The cellular localization of TMEM43 is further complicated by the fact that missense mutations may alter the localization of the protein[23, 28, 29]. Truly understanding where TMEM43 resides within the cell, and whether TMEM43 p.S358L mutation alters this localization is core to our efforts to understand the protein and inform how the pathogenic variant compromises cardiomyocyte function. We tried several different commercially available TMEM43 primary antibodies that had previously been published in immunofluorescence studies[22, 23]. While each of these antibodies worked well for Western blot, unfortunately, none were suitable for immunofluorescence in our hands as demonstrated by equivalent signal intensity in WT and *TMEM43-/-* cells (Supplemental Figure 3). Thus, we were only able to determine a general location for TMEM43 using subcellular fractionation experiments. We found that control and ACM iPSC-CMs express similar levels of TMEM43 which localizes to the membranous protein fraction. The membrane fraction includes many organelles (endoplasmic reticulum, sarcoplasmic reticulum, Golgi apparatus, lysosomes, outer nuclear envelope, etc.) so the precise location of TMEM43 in iPSC-CMs remains unclear. What was clear was that TMEM43 was not present in the nuclear fraction in iPSC-CMs. The nuclear fraction contains the inner nuclear membrane protein lamin, a previously described TMEM43 interacting partner[26]. Future studies will continue to uncover how TMEM43 p.S358L mutation alters

TMEM43 life cycle, subcellular localization, oligomerization and other protein interactions and how these parameters contribute to cardiomyocyte instability.

While ACM caused by TMEM43 p.S358L results in both ventricular arrhythmias and cardiomyopathy, we focused our first study on the pro-arrhythmic tendencies of NL ACM patient iPSC-cardiomyocytes. iPSC-CMs from patients with different types of cardiomyopathy often display abnormal calcium handling, myofibrillar disarray, contractile dysfunction and adipogenic gene expression[30]. Our ACM patient and *TMEM43-/-* iPSC-CMs do not appear to have obvious defects in sarcomere structure, although we did observe a variety of pro-arrhythmic traces in ACM patient iPSC-CMs, including missed contractions and irregularly spaced contractions. However, the most common pro-arrhythmic event we observed was a failure of the calcium to return to baseline, most likely due to early afterdepolarizations. Future studies will examine the electrophysiology of our ACM patient iPSC-CMs to further explore the underlying causes of the observed pro-arrhythmic traces.

We have found that the profound pro-arrhythmic tendencies of ACM iPSC-CMs can be relieved with GSK3 inhibition. Although we observed no difference in phospho-GSK3β (Ser9) or phospho-AKT(Ser473) levels in ACM patient iPSC-CMs relative to control, GSK3 inhibition with CHIR99021 still conferred protection from arrhythmic contractions. GSK3β participates in many signaling pathways that regulate diverse cellular functions including glucose metabolism, protein synthesis, cell mobility, proliferation, survival, and cell fate[31], [32] and other studies have shown beneficial effects of GSK3 inhibition for arrhythmogenic cardiomyopathy models[23, 33, 34]. Indeed, the "Targeted Therapy With Glycogen Synthase Kinase-3 Inhibition for Arrhythmogenic

Cardiomyopathy (TaRGET)" clinical trial will soon begin recruiting ACM patients to evaluate the therapeutic effectiveness of the GSK3β inhibitor tideglusib (https://clinicaltrials.gov/study/NCT06174220).

It is important to note that we believe that our TMEM43 isogenic "repair" iPSC-CMs are not completely functionally restored. Although we genetically repaired the *TMEM43* mutation in severely affected male ACM patient iPSCs, these isogenic control cardiomyocytes continue to exhibit significantly increased contraction frequencies and increased pro-arrhythmic events in response to adrenergic receptor stimulation. Furthermore, GSK3 inhibition showed beneficial effects on these cells as well. Therefore, we speculate that in addition to the TMEM43 p.S358L mutation, there may be other modifiers in these patients that contribute to the severity of their disease. However, further studies using isogenic repair cells from multiple male and female ACM patients are necessary before making a final determination.

Efforts to date within the province of Newfoundland and Labrador have led to an average lifespan increase of 18 years for ACM patients compared to their untreated ancestors[5]. However, ACM caused by TMEM43 p.S358L mutation continues to ravage families and our lack of understanding of the molecular basis of the disease limits our ability to predict disease severity and inform patient treatment options. Future studies will examine the fibrotic or adipogenic gene expression in ACM patient samples, expand the studies to female patients, and try to understand the phenotypic variability in disease presentation and progression.

Conflict of Interest

The authors declare that the research was conducted in the absence of any commercial or financial relationships that could be construed as a potential conflict of interest.

Ethics Statement

The research performed as a part of this study were approved by the Newfoundland and Labrador Human Research Ethics Board # 2020.301 and # 2018.201.

Author Contributions

R.J.N., W.S., C.F., Z.G.P. and H.S. performed experiments and analysed the data. U.B. reprogrammed the iPSCs. D.P. collected the dermal biopsies. T.B. analysed the RNAseq data. K.H. recruited patients and contributed substantive ideas and advice as well as interpretation of the data. J.L.E. oversaw the project. All authors reviewed and edited the manuscript.

Funding

This study was supported by the Stem Cell Network Grant FY21 / ECI-7 and Canadian Institutes for Health Research # 183629 to K.H. and J.L.E.

Acknowledgments

We thank Dr. Dale Laird for generously providing us with the female control iPSCs used in this study and for advice about the electron micrographs. Thank you to Dr. Terry Hébert for introducing us to the Origin software for calcium imaging. We also thank Drs. Stephanie Protze and Bruno Stuyvers for their advice and suggestions. Finally, we

sincerely thank the donors and their families, without whom none of this research would be possible.

Data Availability Statement

The datasets generated during and/or analysed during the current study are available in the GEO repository (XXX)

References

1. Corrado D, Link MS, Calkins H. Arrhythmogenic Right Ventricular Cardiomyopathy. *N Engl J Med* 2017;**376**:1489-1490.
2. Gandjbakhch E, Redheuil A, Pousset F, Charron P, Frank R. Clinical Diagnosis, Imaging, and Genetics of Arrhythmogenic Right Ventricular Cardiomyopathy/Dysplasia: JACC State-of-the-Art Review. *J Am Coll Cardiol* 2018;**72**:784-804.
3. Ohno S. The genetic background of arrhythmogenic right ventricular cardiomyopathy. *J Arrhythm* 2016;**32**:398-403.
4. Stroud MJ. Linker of nucleoskeleton and cytoskeleton complex proteins in cardiomyopathy. *Biophys Rev* 2018;**10**:1033-1051.
5. Hodgkinson KA, Howes AJ, Boland P, Shen XS, Stuckless S, Young TL, Curtis F, Collier A, Parfrey PS, Connors SP. Long-Term Clinical Outcome of Arrhythmogenic Right Ventricular Cardiomyopathy in Individuals With a p.S358L Mutation in TMEM43 Following Implantable Cardioverter Defibrillator Therapy. *Circ Arrhythm Electrophysiol* 2016;**9**.
6. Merner ND, Hodgkinson KA, Haywood AF, Connors S, French VM, Drenckhahn JD, Kupprion C, Ramadanova K, Thierfelder L, McKenna W, Gallagher B, Morris-Larkin L, Bassett AS, Parfrey PS, Young TL. Arrhythmogenic right ventricular cardiomyopathy type 5 is a fully penetrant, lethal arrhythmic disorder caused by a missense mutation in the TMEM43 gene. *Am J Hum Genet* 2008;**82**:809-821.
7. Haywood AF, Merner ND, Hodgkinson KA, Houston J, Syrris P, Booth V, Connors S, Pantazis A, Quarta G, Elliott P, McKenna W, Young TL. Recurrent missense mutations in TMEM43 (ARVD5) due to founder effects cause arrhythmogenic cardiomyopathies in the UK and Canada. *Eur Heart J* 2013;**34**:1002-1011.
8. Milting H, Klauke B, Christensen AH, Müsebeck J, Walhorn V, Grannemann S, Münnich T, Šarić T, Rasmussen TB, Jensen HK, Mogensen J, Baecker C, Romaker E, Laser KT, zu Knyphausen E, Kassner A, Gummert J, Judge DP, Connors S, Hodgkinson K, Young TL, van der Zwaag PA, van Tintelen JP, Anselmetti D. The TMEM43 Newfoundland mutation p.S358L causing ARVC-5 was imported from Europe and increases the stiffness of the cell nucleus. *Eur Heart J* 2015;**36**:872-881.
9. Christensen AH, Andersen CB, Tybjaerg-Hansen A, Haunso S, Svendsen JH. Mutation analysis and evaluation of the cardiac localization of TMEM43 in arrhythmogenic right ventricular cardiomyopathy. *Clin Genet* 2011;**80**:256-264.
10. Hodgkinson KA, Connors SP, Merner N, Haywood A, Young TL, McKenna WJ, Gallagher B, Curtis F, Bassett AS, Parfrey PS. The natural history of a genetic subtype of arrhythmogenic right ventricular cardiomyopathy caused by a p.S358L mutation in TMEM43. *Clin Genet* 2013;**83**:321-331.
11. Calkins H, Corrado D, Marcus F. Risk Stratification in Arrhythmogenic Right Ventricular Cardiomyopathy. *Circulation* 2017;**136**:2068-2082.
12. Sawant AC, Bhonsale A, te Riele AS, Tichnell C, Murray B, Russell SD, Tandri H, Tedford RJ, Judge DP, Calkins H, James CA. Exercise has a disproportionate role in the pathogenesis of arrhythmogenic right ventricular dysplasia/cardiomyopathy in patients without desmosomal mutations. *J Am Heart Assoc* 2014;**3**:e001471.
13. Paulin FL, Hodgkinson KA, MacLaughlan S, Stuckless SN, Templeton C, Shah S, Bremner H, Roberts JD, Young TL, Parfrey PS, Connors SP. Exercise and arrhythmic risk in TMEM43 p.S358L arrhythmogenic right ventricular cardiomyopathy. *Heart Rhythm* 2020.
14. Paix A, Folkmann A, Goldman DH, Kulaga H, Grzelak MJ, Rasoloson D, Paidemarry S, Green R, Reed RR, Seydoux G. Precision genome editing using synthesis-dependent repair of Cas9-induced DNA breaks. *Proc Natl Acad Sci U S A* 2017;**114**:E10745-E10754.

534 15. Baghirova S, Hughes BG, Hendzel MJ, Schulz R. Sequential fractionation and isolation of
535 subcellular proteins from tissue or cultured cells. *MethodsX* 2015;**2**:440-445.
536 16. Laboratory CSH. Mowial-DABCO stock solution. *Cold Spring Harb Protoc* 2007.
537 17. Wingett SW, Andrews S. FastQ Screen: A tool for multi-genome mapping and quality control.
538 *F1000Res* 2018;**7**:1338.
539 18. Dobin A, Davis CA, Schlesinger F, Drenkow J, Zaleski C, Jha S, Batut P, Chaisson M, Gingeras TR.
540 STAR: ultrafast universal RNA-seq aligner. *Bioinformatics* 2013;**29**:15-21.
541 19. Liao Y, Smyth GK, Shi W. featureCounts: an efficient general purpose program for assigning
542 sequence reads to genomic features. *Bioinformatics* 2014;**30**:923-930.
543 20. Love MI, Huber W, Anders S. Moderated estimation of fold change and dispersion for RNA-seq
544 data with DESeq2. *Genome Biol* 2014;**15**:550.
545 21. Young MD, Wakefield MJ, Smyth GK, Oshlack A. Gene ontology analysis for RNA-seq: accounting
546 for selection bias. *Genome Biol* 2010;**11**:R14.
547 22. Jang MW, Oh DY, Yi E, Liu X, Ling J, Kim N, Sharma K, Kim TY, Lee S, Kim AR, Kim MY, Kim MA, Lee
548 M, Han JH, Han JJ, Park HR, Kim BJ, Lee SY, Woo DH, Oh J, Oh SJ, Du T, Koo JW, Oh SH, Shin HW,
549 Seong MW, Lee KY, Kim UK, Shin JB, Sang S, Cai X, Mei L, He C, Blanton SH, Chen ZY, Chen H,
550 Nourbakhsh A, Huang Z, Kang KW, Park WY, Feng Y, Lee CJ, Choi BY. A nonsense. *Proc Natl Acad*
551 *Sci U S A* 2021;**118**.
552 23. Padrón-Barthe L, Villalba-Orero M, Gómez-Salinero JM, Domínguez F, Román M, Larrasa-Alonso
553 J, Ortiz-Sánchez P, Martínez F, López-Olañeta M, Bonzón-Kulichenko E, Vázquez J, Martí-Gómez
554 C, Santiago DJ, Prados B, Giovinazzo G, Gómez-Gaviro MV, Priori S, Garcia-Pavia P, Lara-Pezzi E.
555 Severe Cardiac Dysfunction and Death Caused by Arrhythmogenic Right Ventricular
556 Cardiomyopathy Type 5 Are Improved by Inhibition of Glycogen Synthase Kinase-3β. *Circulation*
557 2019;**140**:1188-1204.
558 24. Etchegary H, Pullman D, Simmonds C, Young TL, Hodgkinson K. 'It had to be done': genetic testing
559 decisions for arrhythmogenic right ventricular cardiomyopathy. *Clin Genet* 2015;**88**:344-351.
560 25. Elliott PM, Anastasakis A, Asimaki A, Basso C, Bauce B, Brooke MA, Calkins H, Corrado D, Duru F,
561 Green KJ, Judge DP, Kelsell D, Lambiase PD, McKenna WJ, Pilichou K, Protonotarios A, Saffitz JE,
562 Syrris P, Tandri H, Te Riele A, Thiene G, Tsatsopoulou A, van Tintelen JP. Definition and treatment
563 of arrhythmogenic cardiomyopathy: an updated expert panel report. *Eur J Heart Fail* 2019.
564 26. Bengtsson L, Otto H. LUMA interacts with emerin and influences its distribution at the inner
565 nuclear membrane. *J Cell Sci* 2008;**121**:536-548.
566 27. Franke WW, Dörflinger Y, Kuhn C, Zimbelmann R, Winter-Simanowski S, Frey N, Heid H. Protein
567 LUMA is a cytoplasmic plaque constituent of various epithelial adherens junctions and composite
568 junctions of myocardial intercalated disks: a unifying finding for cell biology and cardiology. *Cell*
569 *Tissue Res* 2014;**357**:159-172.
570 28. Siragam V, Cui X, Masse S, Ackerley C, Aafaqi S, Strandberg L, Tropak M, Fridman MD,
571 Nanthakumar K, Liu J, Sun Y, Su B, Wang C, Liu X, Yan Y, Mendlowitz A, Hamilton RM. TMEM43
572 mutation p.S358L alters intercalated disc protein expression and reduces conduction velocity in
573 arrhythmogenic right ventricular cardiomyopathy. *PLoS One* 2014;**9**:e109128.
574 29. Shinomiya H, Kato H, Kuramoto Y, Watanabe N, Tsuruda T, Arimura T, Miyashita Y, Miyasaka Y,
575 Mashimo T, Takuwa A, Motooka D, Okuzaki D, Matsuoka K, Tsukamoto O, Hakui H, Yamada N, Lee
576 JK, Kioka H, Kitakaze M, Takashima S, Sakata Y, Asano Y. Aberrant accumulation of TMEM43
577 accompanied by perturbed transmural gene expression in arrhythmogenic cardiomyopathy.
578 *FASEB J* 2021;**35**:e21994.
579 30. Musunuru K, Sheikh F, Gupta RM, Houser SR, Maher KO, Milan DJ, Terzic A, Wu JC, Biology
580 AHACoFGaT, Young CoCDit, Nursing aCoCaS. Induced Pluripotent Stem Cells for Cardiovascular

581 Disease Modeling and Precision Medicine: A Scientific Statement From the American Heart
582 Association. *Circ Genom Precis Med* 2018;**11**:e000043.
583 31. Beurel E, Grieco SF, Jope RS. Glycogen synthase kinase-3 (GSK3): regulation, actions, and diseases.
584 *Pharmacol Ther* 2015;**148**:114-131.
585 32. Wang L, Li J, Di LJ. Glycogen synthesis and beyond, a comprehensive review of GSK3 as a key
586 regulator of metabolic pathways and a therapeutic target for treating metabolic diseases. *Med*
587 *Res Rev* 2022;**42**:946-982.
588 33. Chelko SP, Asimaki A, Andersen P, Bedja D, Amat-Alarcon N, DeMazumder D, Jasti R, MacRae CA,
589 Leber R, Kleber AG, Saffitz JE, Judge DP. Central role for GSK3β in the pathogenesis of
590 arrhythmogenic cardiomyopathy. *JCI Insight* 2016;**1**.
591 34. Khudiakov A, Zaytseva A, Perepelina K, Smolina N, Pervunina T, Vasichkina E, Karpushev A, Tomilin
592 A, Malashicheva A, Kostareva A. Sodium current abnormalities and deregulation of Wnt/β-catenin
593 signaling in iPSC-derived cardiomyocytes generated from patient with arrhythmogenic
594 cardiomyopathy harboring compound genetic variants in plakophilin 2 gene. *Biochim Biophys*
595 *Acta Mol Basis Dis* 2020;**1866**:165915.

596

Figure legends

Figure 1. ACM patient iPSC-cardiomyocytes exhibit pro-arrhythmic tendencies. (A) Representative Fluo4 traces demonstrating calcium handling in unstimulated iPSC-CMs after 4 weeks of contraction in culture. **(B)** Contractions per minute in unstimulated iPSC-CMs. **(C)** Blinded scoring of calcium image tracing. Traces were scored either as “normal”, pro-arrhythmic” (Arrhyth.) or “not determined” (N.D). **(D)** Quantified parameters associated with calcium traces. **(E)** Average calcium peak shape as determined by overlaying all peaks. Data representative of 3-8 independent experiments, comprising 29-63 individual calcium traces for each cell line. n.s, not significant; *, $p < 0.05$; **, $p < 0.01$; ***, $p < 0.001$; ****, $p < 0.0001$.

Figure 2. Isoproterenol exacerbates the pro-arrhythmic tendencies of isogenic repair patient iPSC-cardiomyocytes. (A) Representative Fluo4 traces demonstrating calcium handling iPSC-CMs stimulated with 10 µM isoproterenol. **(B)** Quantified parameters associated with calcium traces in isoproterenol-stimulated iPSC-CMs. **(C)** Blinded scoring of calcium image tracing. Traces were scored either as “normal”, pro-arrhythmic” (Arrhyth.) or “not determined” (N.D). Data representative of 2-5 independent experiments, comprising 18-55 individual calcium traces for each cell line. *, $p < 0.05$; **, $p < 0.01$; ***, $p < 0.001$; ****, $p < 0.0001$.

Figure 3. Expression, half-life and subcellular distribution of key intracellular proteins is unchanged in ACM iPSC-cardiomyocytes. (A) Representative Western blot and **(B)** densitometric quantification of TMEM43 protein abundance in control or ACM patient iPSC-CMs. **(C)** Representative Western blot and **(D)** densitometric analysis of

TMEM43 and Cx43 protein expression in control and ACM patient iPSC-CMs treated with the protein synthesis inhibitor cycloheximide. **(E)** Subcellular fractionation demonstrating typical subcellular distribution of several intracellular proteins in unaffected control and ACM patient iPSC-CMs. **(F)** Densitometric quantification of total Cx43 protein abundance and the proportion of phosphoylated “P2” and “P1” Cx43 species compared to unphosphoylated “P0” Cx43 in control and ACM patient iPSC-CMs. Data represent the standard error of the mean of 3-4 independent experiments. n.s. not significant.

Figure 4. ACM patient iPSC-cardiomyocytes exhibit typical cellular organelle morphology. (A) Representative transmission electron micrographs and **(B)** representative immunofluorescence confocal micrographs of various intracellular organelle markers (green) in unaffected control and ACM patient iPSC-cardiomyocytes. Nuclei (Hoechst, blue). Scale bars as indicated. ER, endoplasmic reticulum; NE, nuclear envelope; Nu, nucleus; D, desmosome; Z, Z-disc; M, mitochondria.

Figure 5. AKT signaling pathway unperturbed in ACM iPSC-cardiomyocytes. (A) Representative Western blots and **(B)** densitometric analysis of various signaling molecules in unaffected control and ACM patient iPSC-CMs. Data represent the standard error of the mean of 4 independent experiments.

Figure 6. Altered gene expression related to metabolism and signaling in ACM patient iPSC-cardiomyocytes. (A) Venn diagram depicting sample comparisons. We compared ACM patient iPSC-CMs to unaffected familial control after filtering for genes that were common between the ACM patient and the isogenic control samples. **(B)** The volcano plot illustrates the top differentially expressed genes where $\log_2$ fold change is >|1|. 492 genes were up-regulated and 82 genes were down-regulated. **(C)** KEGG

pathway analysis for significant differentially expressed genes (DEG) in ACM patient iPSC-CMs. **(D)** GoSeq plot showing the top over-represented categories in molecular function. **(E)** GoSeq plot showing the top over-represented categories in biological processes. **(F)** GoSeq plot showing the top over-represented categories in cellular components.

Figure 7. ACM iPSC-cardiomyocyte pro-arrhythmic tendencies can be ameliorated with GSK3 inhibition. (A, B) Representative Fluo4 traces demonstrating calcium handling in ACM patient iPSC-CMs treated with 2 µM of the GSK3 inhibitor CHIR99021. **(C)** Blinded scoring of calcium image tracing. Traces were scored either as “normal”, pro-arrhythmic” (Arrhyth.) or “not determined” (N.D). **(D)** Quantified parameters associated with calcium traces in CHIR-treated ACM patient iPSC-CMs. **(E)** Average calcium peak shape of CHIR-treated ACM patient iPSC-CMs. **(F, G)** Representative Fluo4 traces demonstrating calcium handling in isogenic “repair” iPSC-CMs treated with 2 µM of the GSK3 inhibitor CHIR99021. **(H)** Blinded scoring of calcium image tracing. Traces were scored either as “normal”, arrhythmogenic” or “undetermined”. **(I)** Quantified parameters associated with calcium traces in CHIR99021-treated isogenic repair iPSC-CMs. **(J)** Average calcium peak shape of CHIR-treated isogenic repair iPSC-CMs. Data representative of 3 independent experiments, comprising 24-34 individual calcium traces for each cell line. n.s., not significant; ***, $p < 0.001$; ****, $p < 0.0001$ compared to untreated.

Supplemental Figure 1. iPSCs, CRISPR gene editing, and cardiac differentiation. (A) Representative phase contrast micrograph demonstrating typical morphology of iPSCs reprogrammed from control and ACM patient donors. **(B)** Representative flow

cytometric plot showing high expression of key pluripotency markers in our iPSCs. **(C)** Representative immunoblot demonstrating the absence of the TMEM43 protein in iPSCs after CRISPR-Cas9 gene ablation. **(D)** Gene schematic and Sanger Sequencing result of unaffected control, ACM patient and CRISPR-Cas9 isogenic repair iPSCs. In addition to repairing the C>T transition, the repair template included silent mutations to destroy the CRISPR PAM site (eliminate repeated Cas9 cutting) and delete a restriction enzyme cut site (facilitate screening). **(E)** Representative immunofluorescence confocal micrographs demonstrating cTNT and MLC2V expression in our differentiated iPSC-cardiomyocytes. **(F, G)** Representative flow cytometric plot and associated quantification of the proportion of cTNT expressing cells after iPSC-cardiomyocyte differentiation.

Supplemental Figure 2. TMEM43 is a relatively long-lived protein, resides in the membrane fraction and self-oligomerizes. Representative Western blot and densitometric analysis of TMEM43 and Cx43 protein expression in **(A, Ai)** wild type AD293 cells and **(B, Bi)** undifferentiated control iPSCs treated with cycloheximide. Data represent the standard error of the mean of 3-4 independent experiments. **(C)** Co-immunoprecipitation demonstrates oligomerization of the wild type and S358L mutant TMEM43 protein in transfected AD293 cells. **(D)** Subcellular fractionation demonstrating TMEM43 localization to the membrane compartment in undifferentiated control iPSCs.

Supplemental Figure 3. TMEM43 antibodies work well for WB, but are unsuitable for IF. (A) Representative Western blot and **(B)** representative immunofluorescence confocal micrograph of TMEM43 protein expression in WT and *TMEM43-/-* iPSCs. **(C)** Representative immunofluorescence confocal micrograph of iPSCs overexpressing

TMEM43-FLAG. Nuclei (Hoechst, blue); Flag tag (Red); TMEM43 ab184164 (abcam, green); TMEM43 sc-271887 (Santa Cruz, purple). Scale bars as indicated.

Supplemental Figure 4. ACM patient iPSC-cardiomyocytes exhibit typical cellular organelle morphology. (A) Quantification of the distance between Z-discs in control and ACM patient iPSC-cardiomyocytes. Measurements were made using electron microscopy images. **(B)** Representative flow cytometric analysis plots for cleaved capsase 3 (CC3; marker of apoptosis) in unaffected control and ACM patient iPSC-cardiomyocytes.

Supplemental Figure 5. *TMEM43-/-* iPSC-cardiomyocytes exhibit typical cellular organelle morphology. Representative immunofluorescence confocal micrographs of various intracellular organelle markers (green) in wild type and *TMEM43-/-* iPSC-cardiomyocytes. Nuclei (Hoechst, blue). Scale bar = 10 μm.

Supplemental Videos 1 & 2. Phase contrast movies of contracting iPSC-cardiomyocytes generated from severely affected male ACM patient and unaffected sibling control.

Supplemental Video 3, 4 & 5. Pseudo-coloured Fluo4 calcium fluorescence time-lapse videos of contracting iPSC-cardiomyocytes generated from 2 severely affected male ACM patients and one unaffected sibling control. Scale bar as indicated

Figure 1) ACM patient iPSC-cardiomyocytes exhibit pro-arrhythmic tendencies

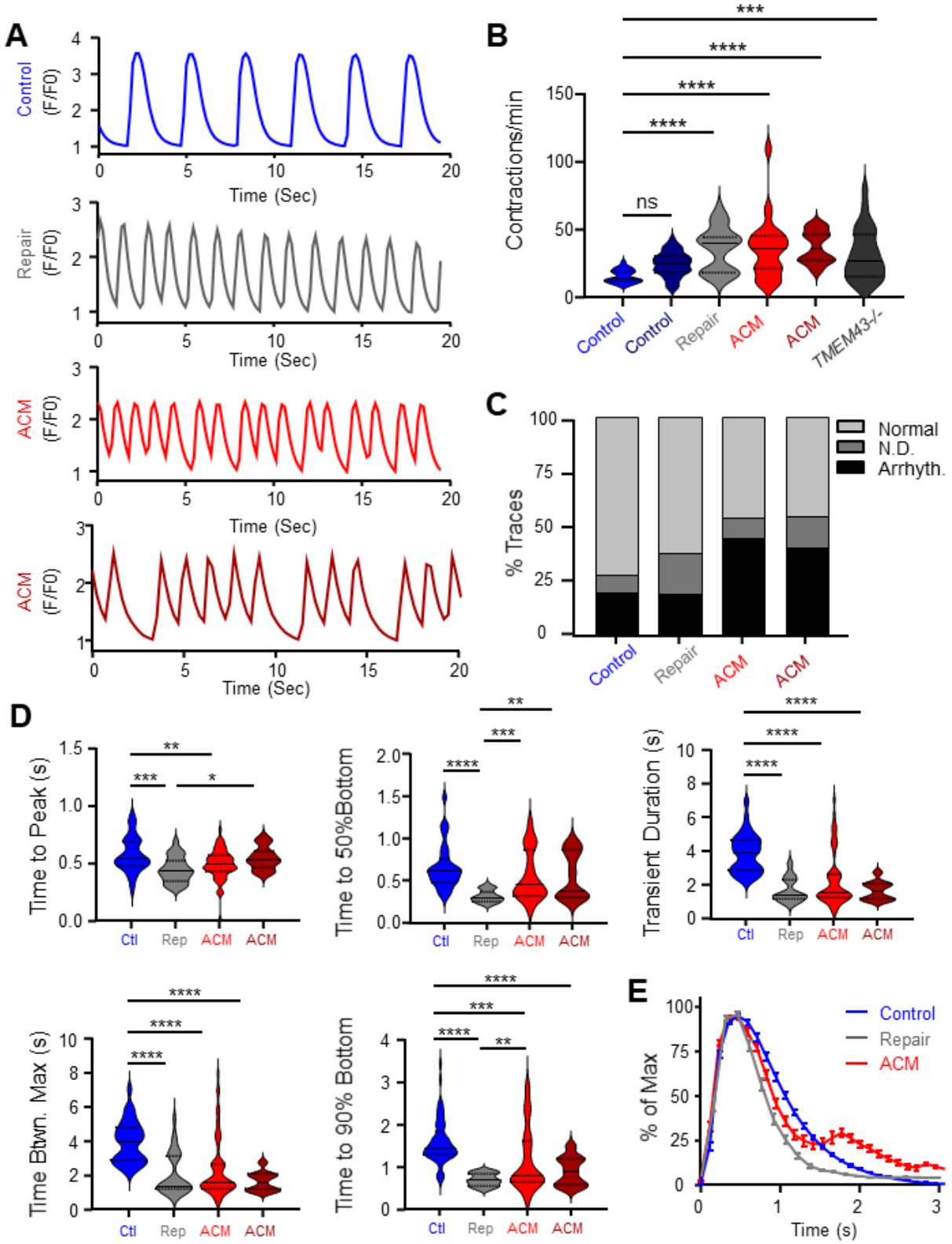

706

Figure 2) Isoproterenol exacerbates the pro-arrhythmic tendencies of isogenic repair patient iPSC-cardiomyocytes

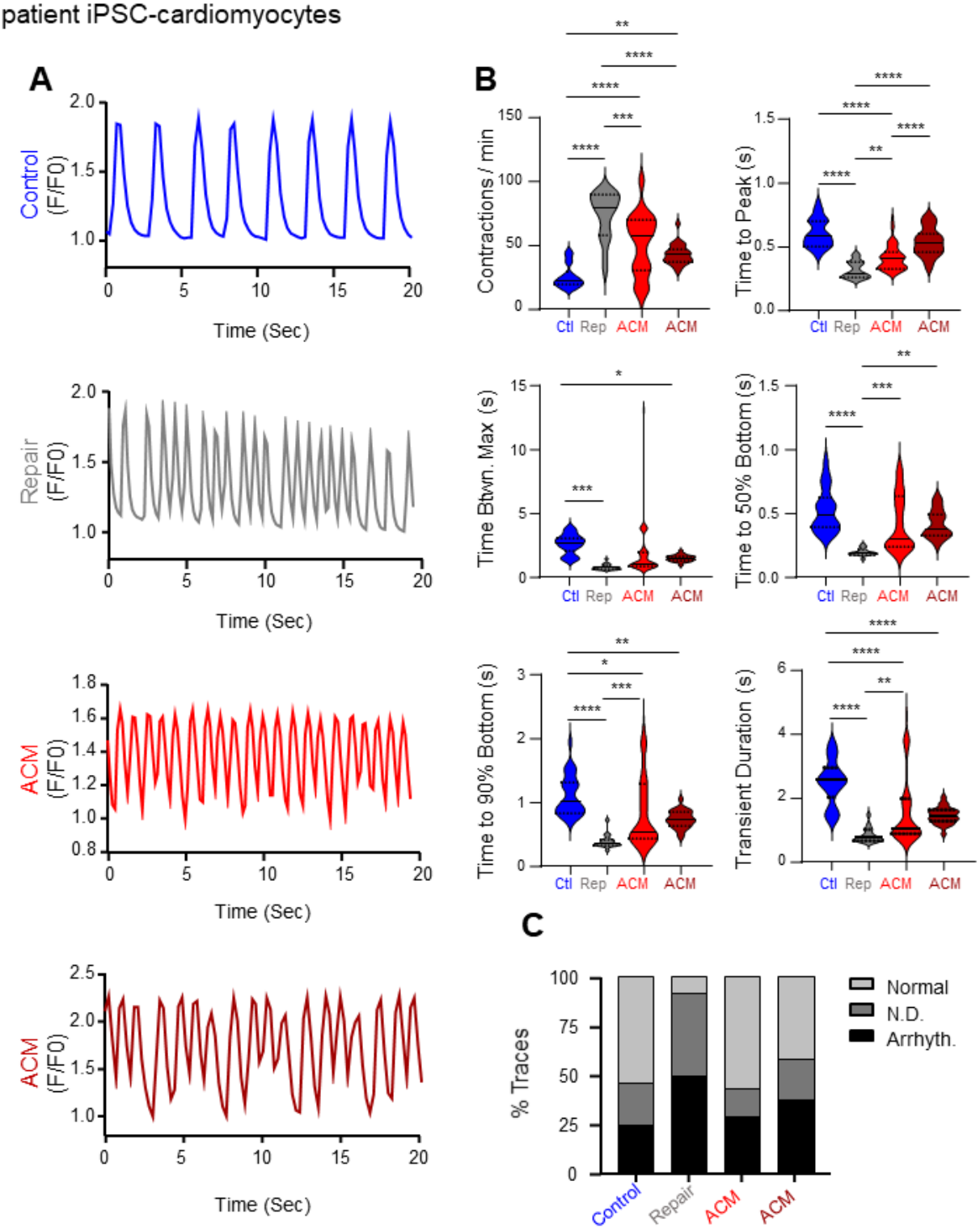

Figure 3) Expression, half-life and subcellular distribution of key intracellular proteins is unchanged in ACM iPSC-CMs

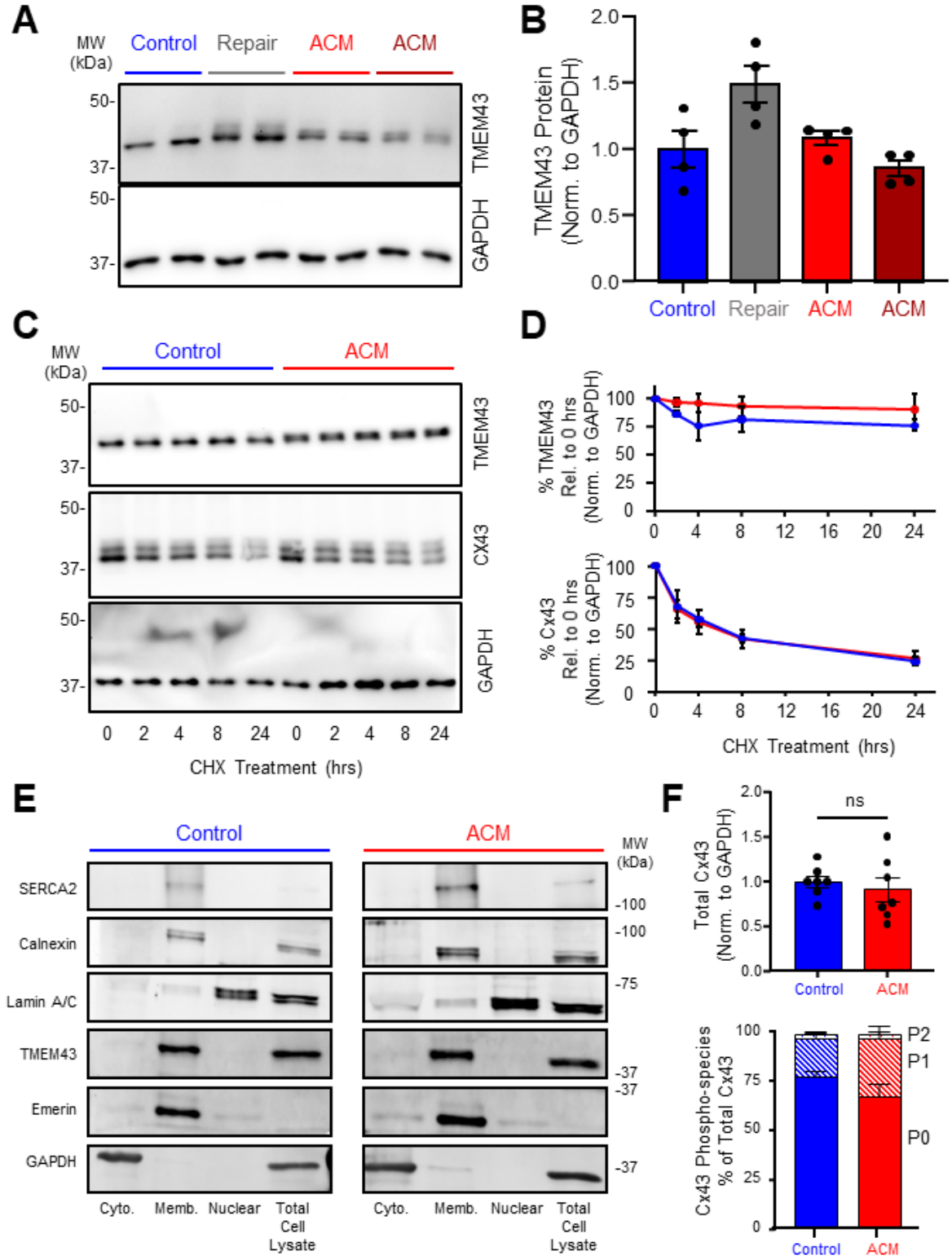

708

Figure 4) ACM patient iPSC-CMs exhibit typical cellular organelle morphology

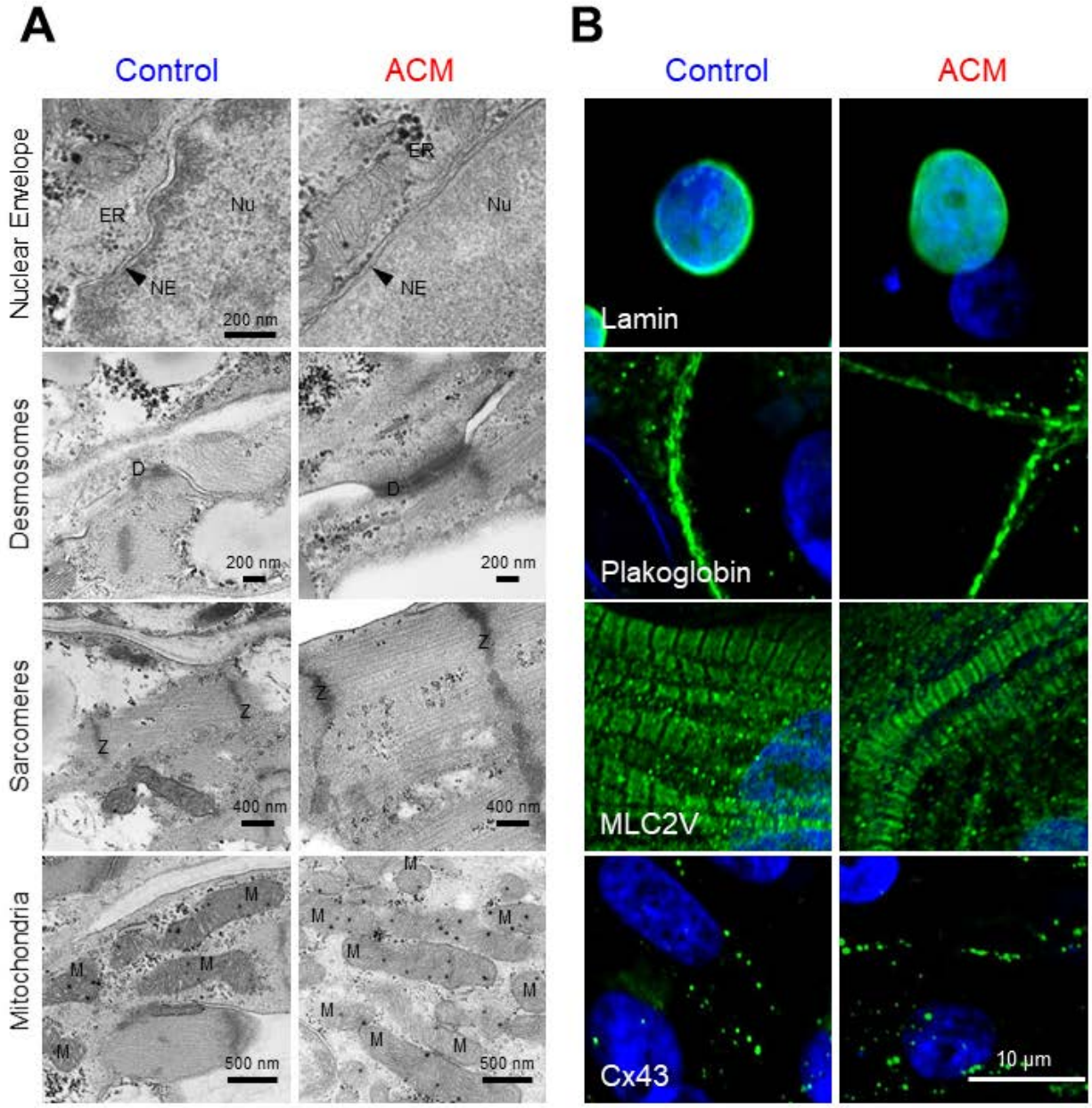

Figure 5) AKT signaling pathway unperturbed in ACM5 iPSC-CMs

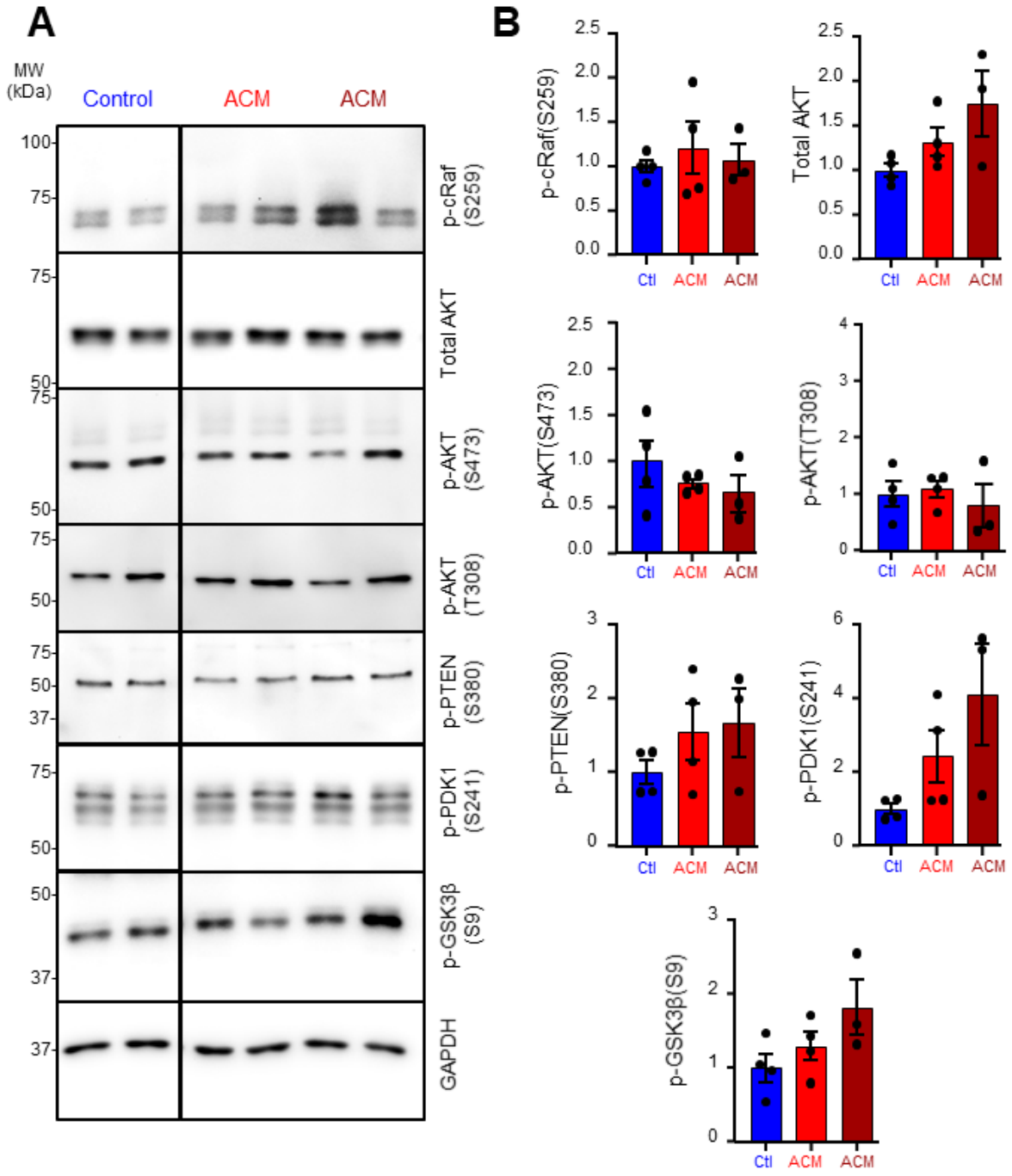

710

Figure 6) Altered gene expression related to metabolism and signaling in ACM patient iPSC-cardiomyocytes.

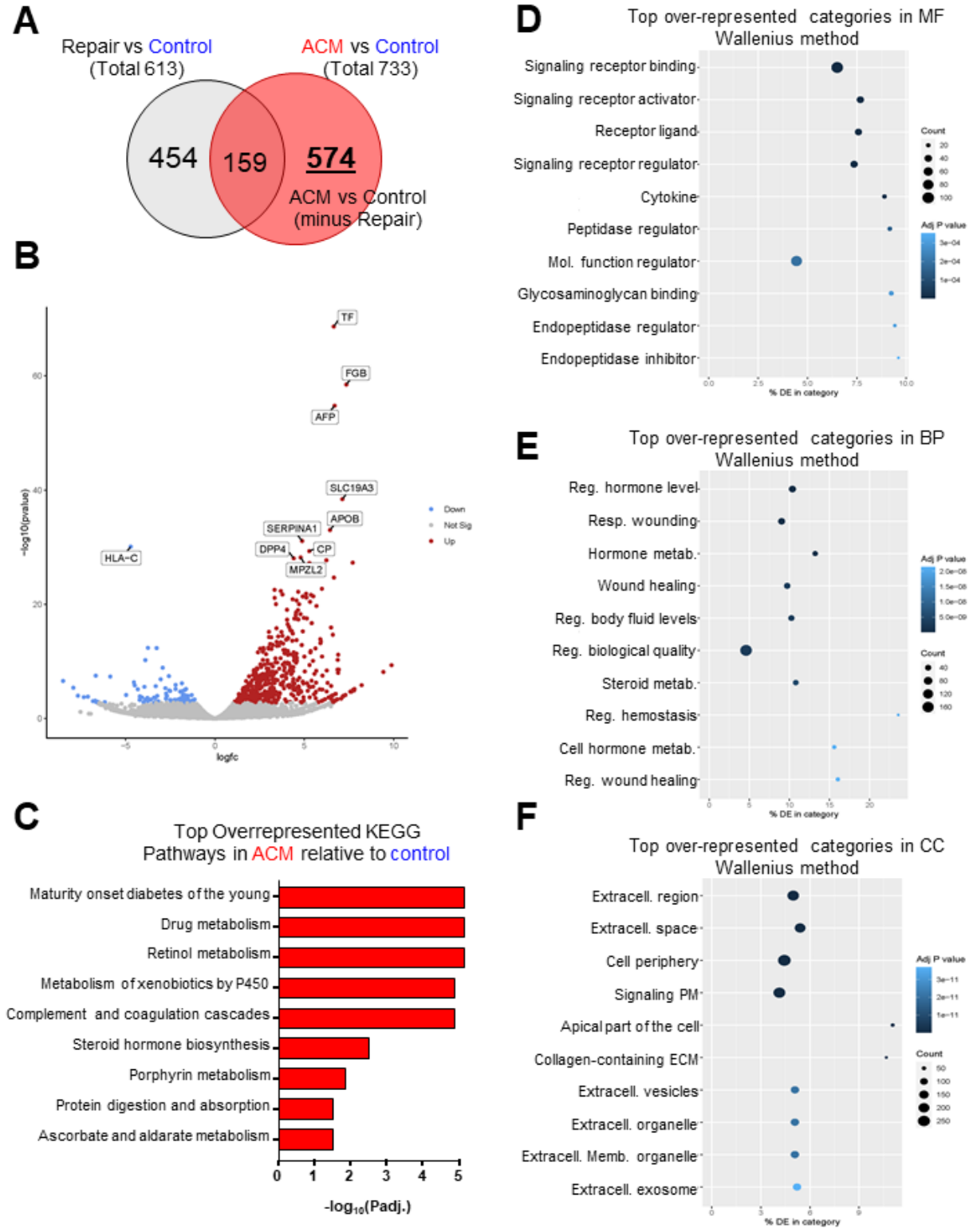

711

Figure 7) ACM iPSC-CM pro-arrhythmic tendencies can be ameliorated with GSK3 inhibition

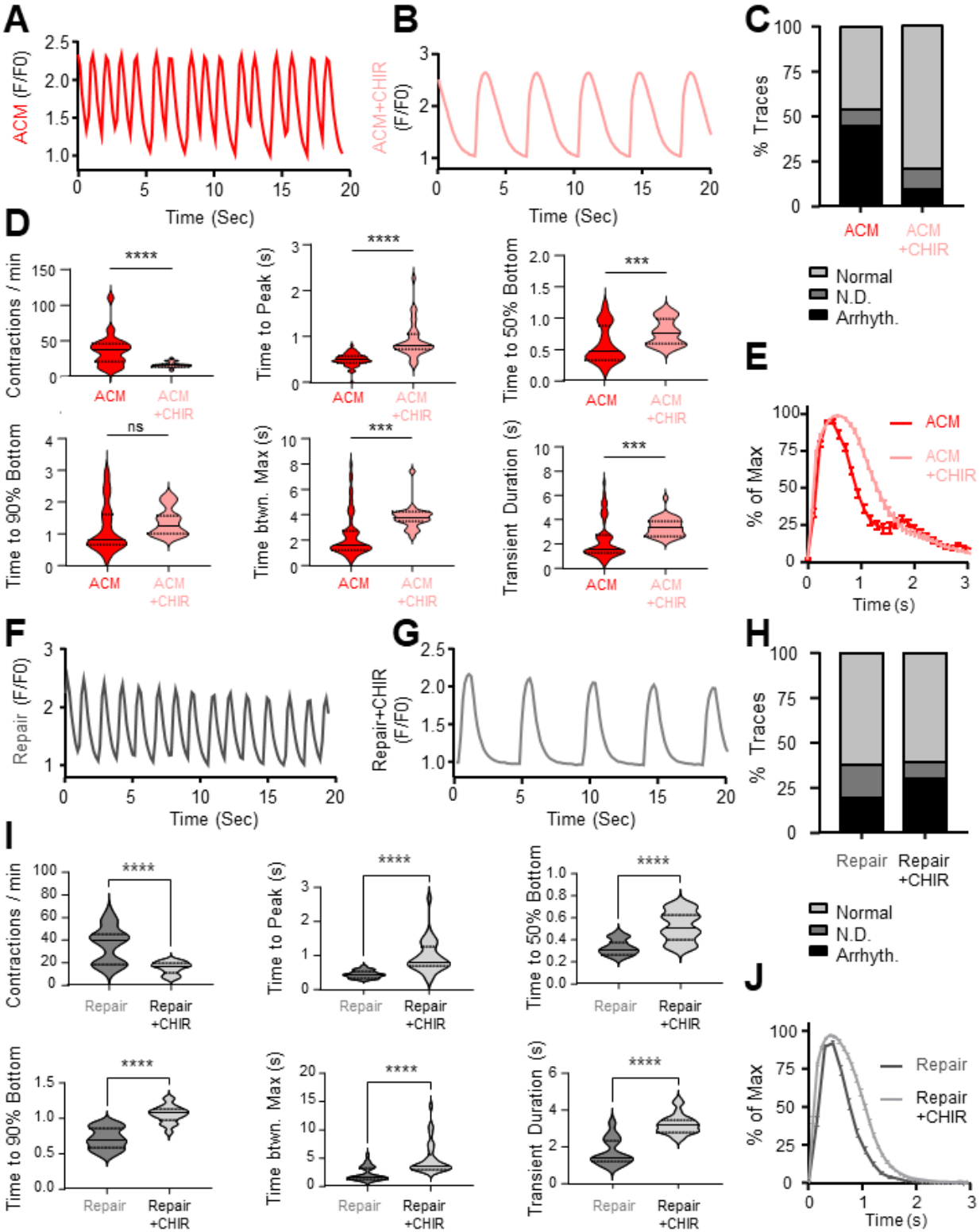

712

Supplemental Figure 1) iPSCs, CRISPR Gene Editing, and Cardiac Differentiation

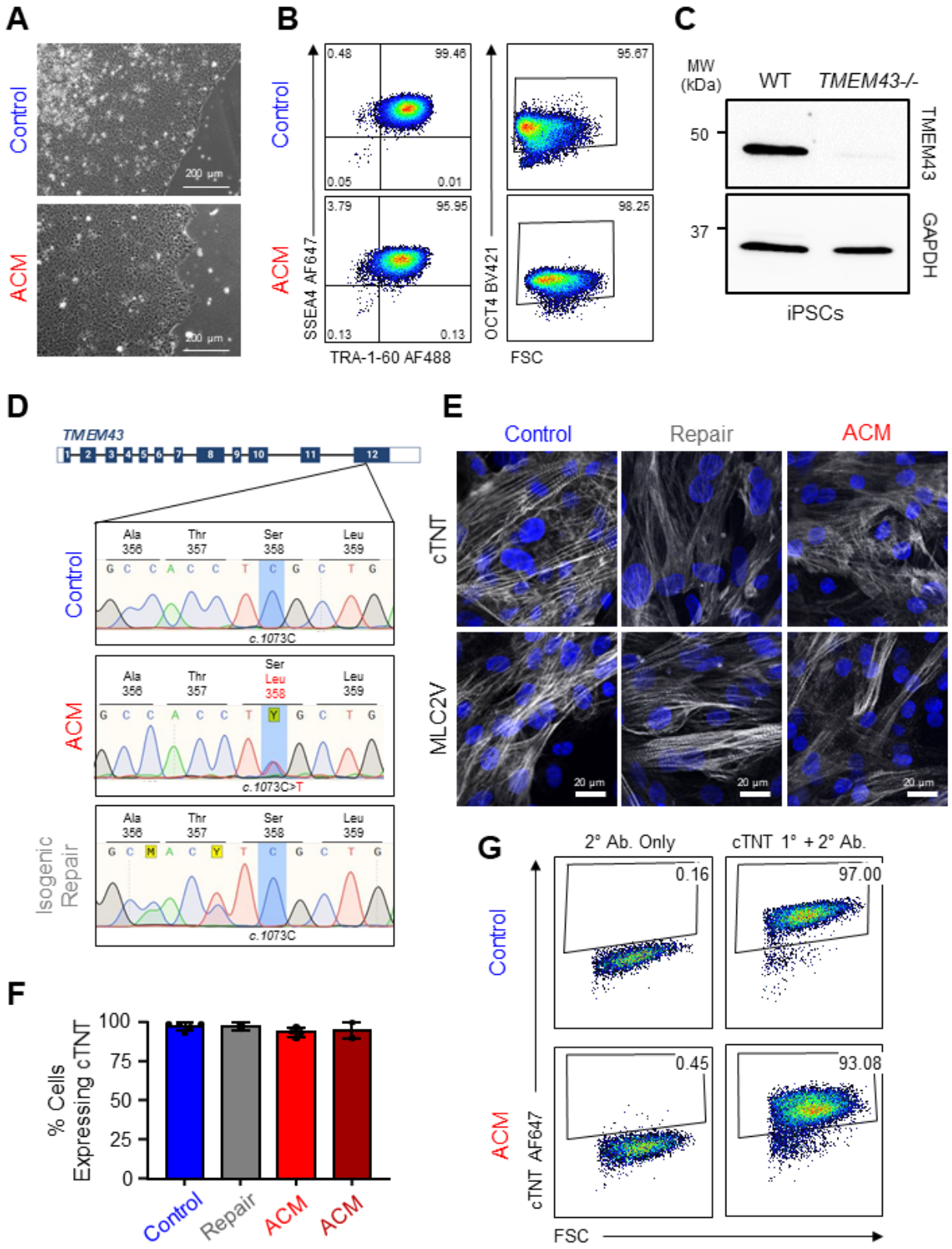

713

Supplemental Figure 2) TMEM43 is a relatively long-lived protein, resides in the membrane fraction and self-oligomerizes

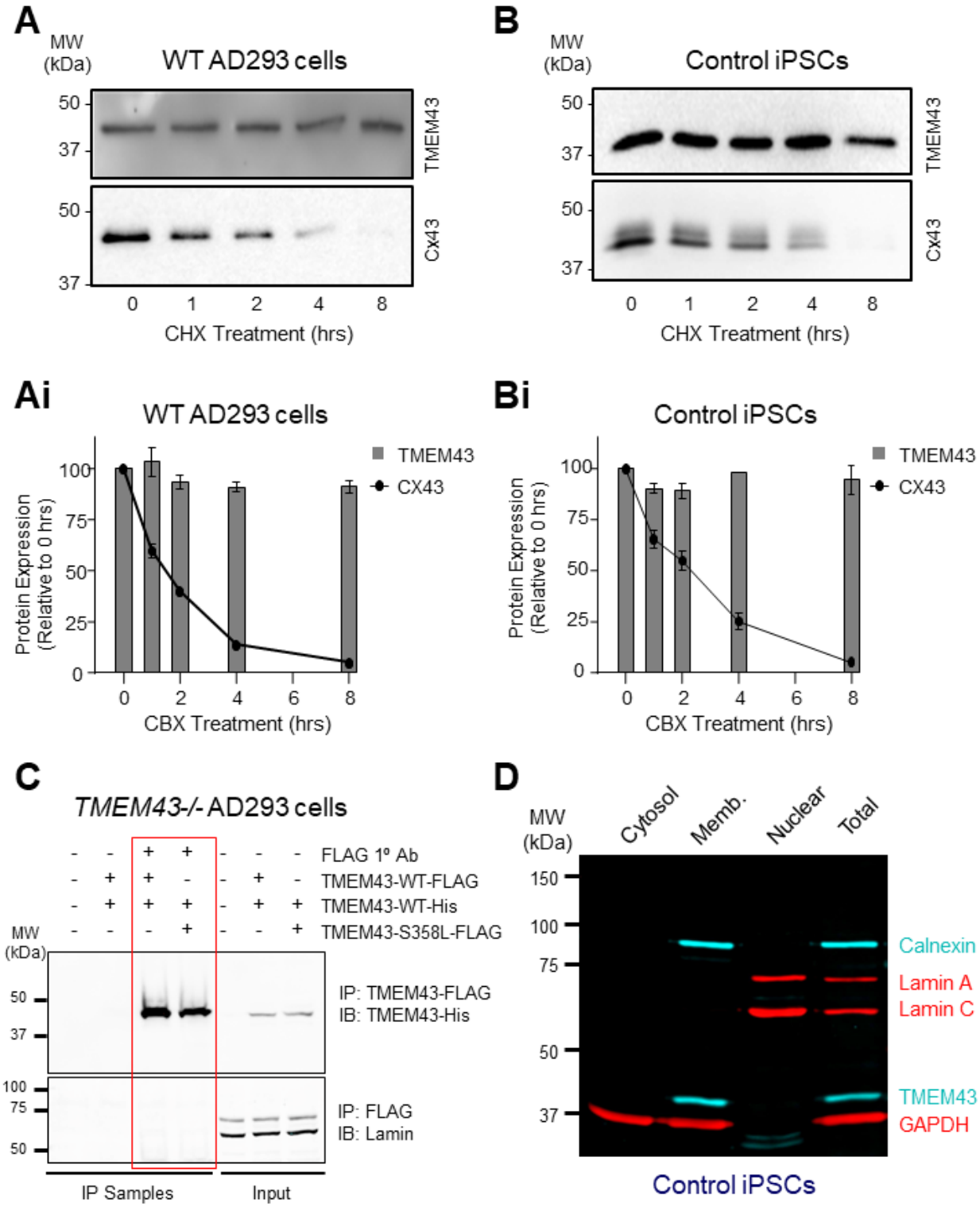

714

Supplementary Figure 3) TMEM43 antibodies work well for WB, but are unsuitable for IF

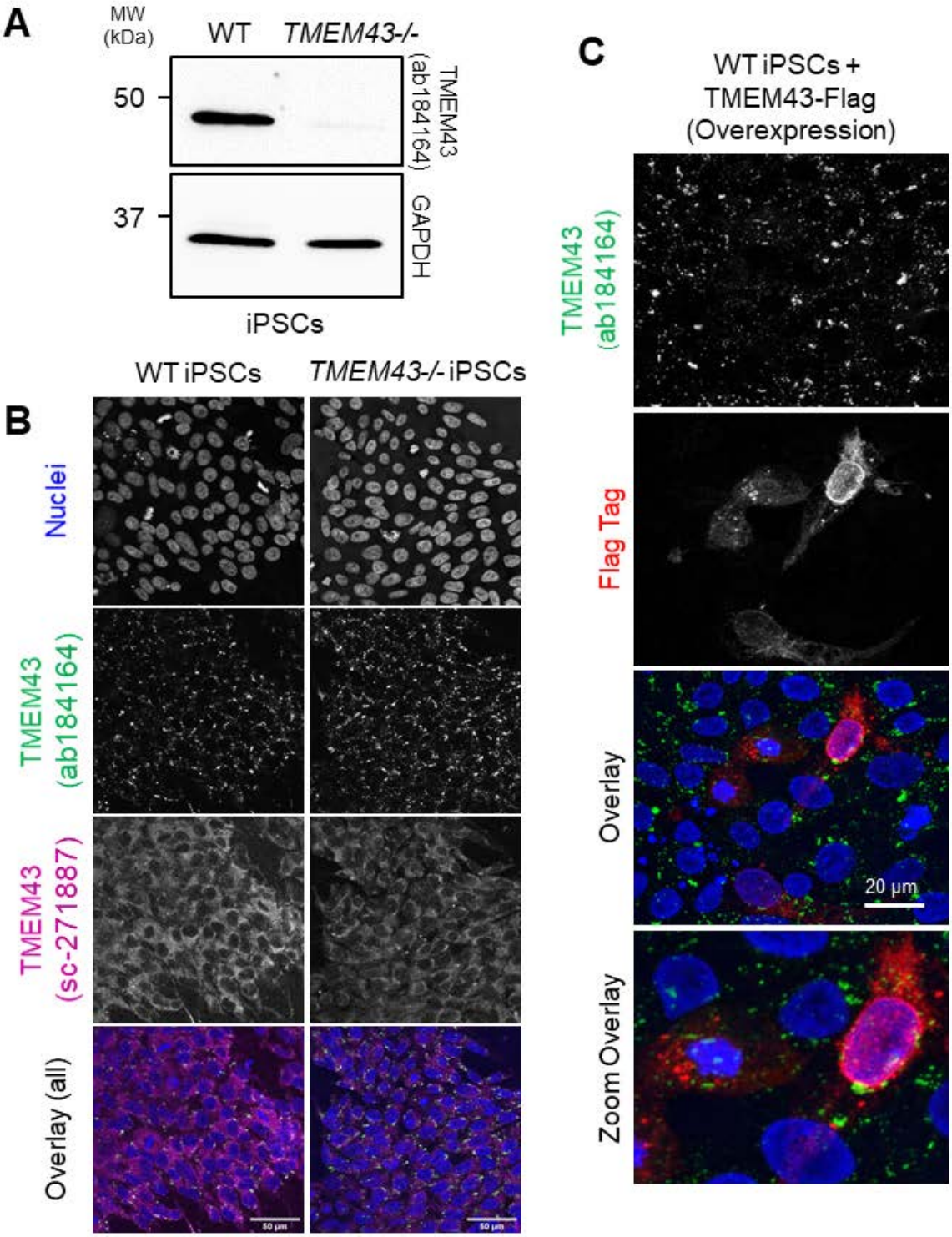

715

Supplemental Figure 4) ACM patient iPSC-CMs exhibit typical cellular organelle morphology

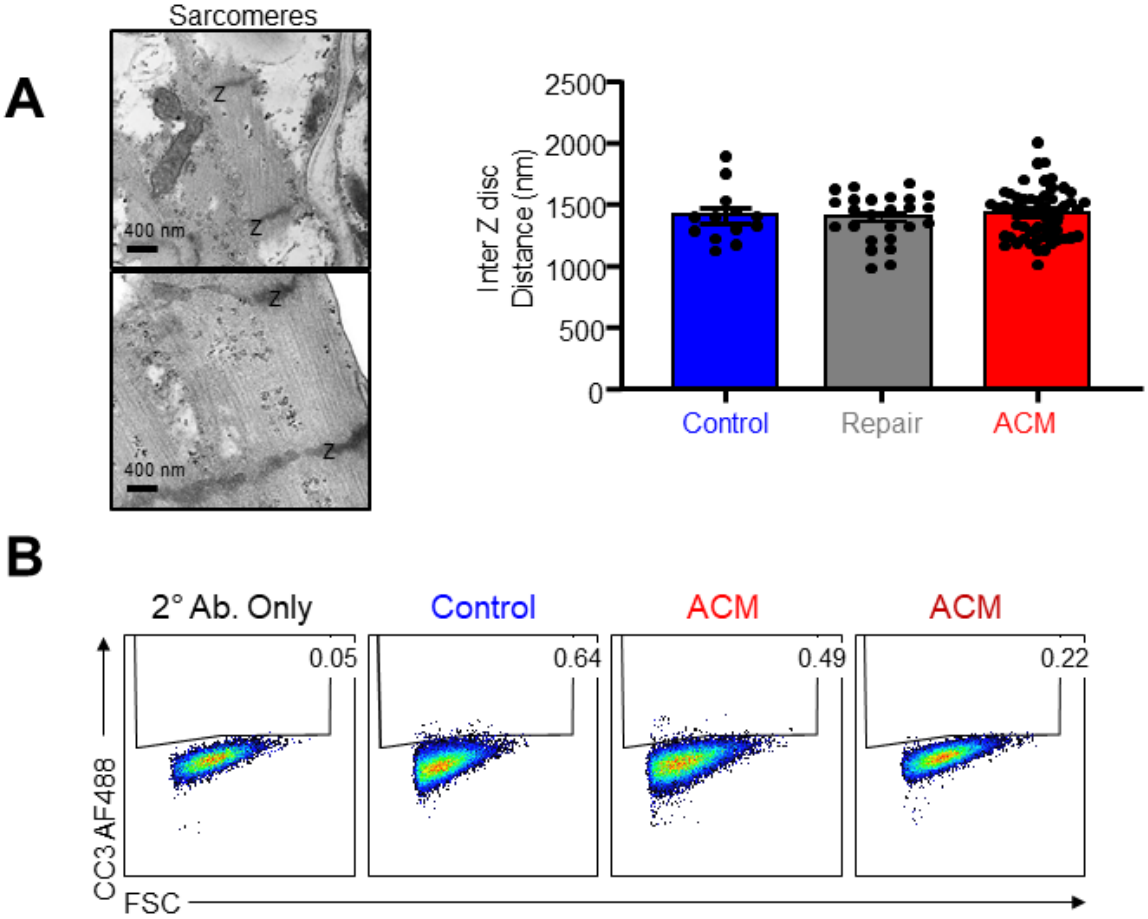

Supplemental Figure 5) *TMEM43-/-* iPSC-CMs exhibit typical cellular organelle morphology

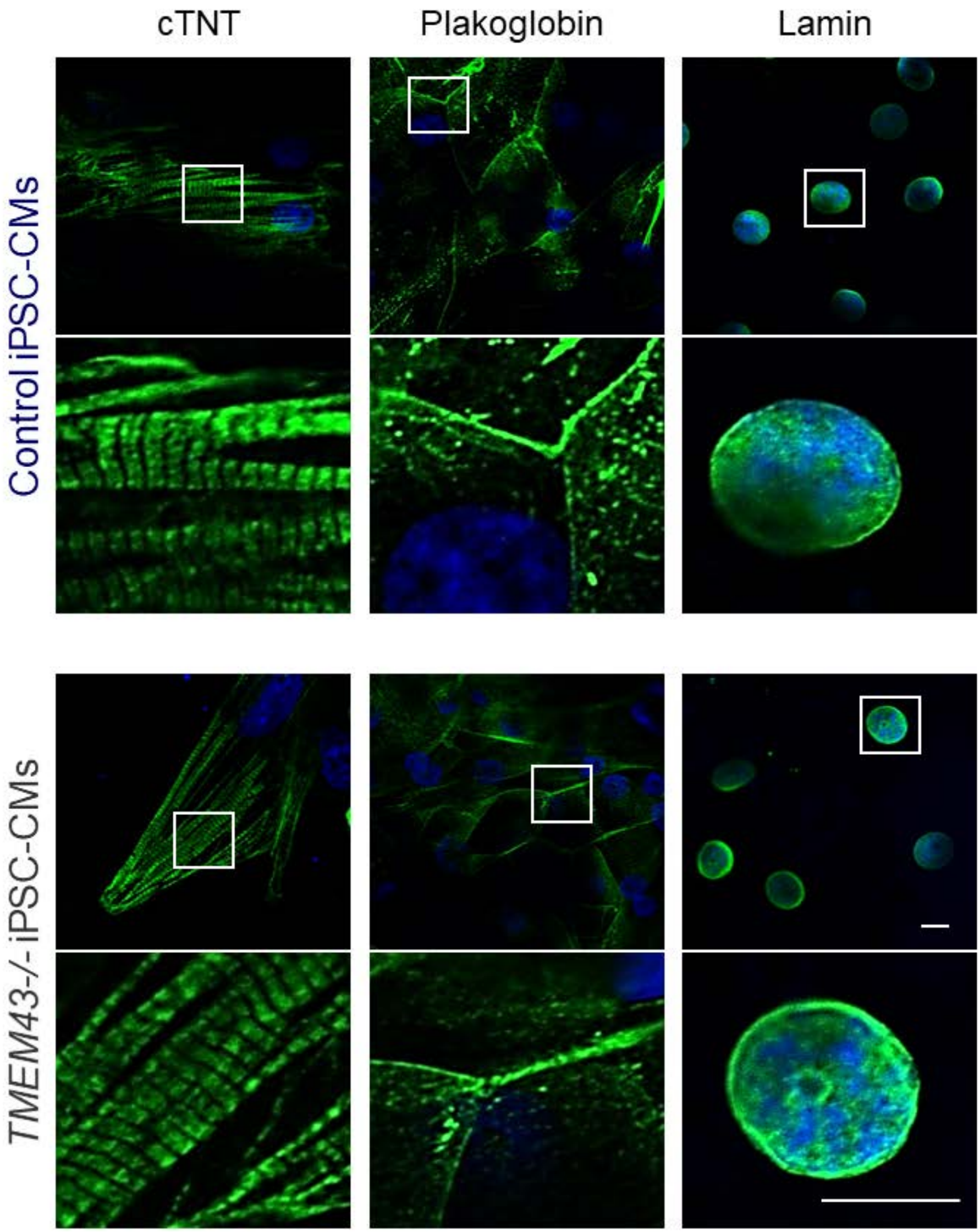

717